1988

Diagnostic and normalization techniques for laser-generated plumes based on beam deflection and photoacoustic wave measurements

Guoying Chen
Iowa State University

3

89

09134

INFORMATION TO USERS

The most advanced technology has been used to photograph and reproduce this manuscript from the microfilm master. UMI films the text directly from the original or copy submitted. Thus, some thesis and dissertation copies are in typewriter face, while others may be from any type of computer printer.

The quality of this reproduction is dependent upon the quality of the copy submitted. Broken or indistinct print, colored or poor quality illustrations and photographs, print bleedthrough, substandard margins, and improper alignment can adversely affect reproduction.

In the unlikely event that the author did not send UMI a complete manuscript and there are missing pages, these will be noted. Also, if unauthorized copyright material had to be removed, a note will indicate the deletion.

Oversize materials (e.g., maps, drawings, charts) are reproduced by sectioning the original, beginning at the upper left-hand corner and continuing from left to right in equal sections with small overlaps. Each original is also photographed in one exposure and is included in reduced form at the back of the book. These are also available as one exposure on a standard 35mm slide or as a 17" x 23" black and white photographic print for an additional charge.

Photographs included in the original manuscript have been reproduced xerographically in this copy. Higher quality 6" x 9" black and white photographic prints are available for any photographs or illustrations appearing in this copy for an additional charge. Contact UMI directly to order.

U·M·I

University Microfilms International
A Bell & Howell Information Company
300 North Zeeb Road, Ann Arbor, MI 48106-1346 USA
313/761-4700 800/521-0600

Order Number 8909134

Diagnostic and normalization techniques for laser-generated plumes based on beam deflection and photoacoustic wave measurements

Chen, Guoying, Ph.D.

Iowa State University, 1988

U·M·I
300 N. Zeeb Rd.
Ann Arbor, MI 48106

Diagnostic and normalization techniques for laser-generated plumes based on beam deflection and photoacoustic wave measurements

by

Guoying Chen

A Dissertation Submitted to the
Graduate Faculty in Partial Fulfillment of the
Requirements for the Degree of
DOCTOR OF PHILOSOPHY

Department: Chemistry
Major: Analytical Chemistry

Approved:

Signature was redacted for privacy.

In Charge of Major Work

Signature was redacted for privacy.

For the Major Department

Signature was redacted for privacy.

For the Graduate College

Iowa State University
Ames, Iowa

1988

TABLE OF CONTENTS

TABLE OF FIGURES

Page

Page

GENERAL INTRODUCTION

Introduction to Laser Microprobe Analysis

Detection of trace elements in industrial, medical, biological and environmental materials has become a major analytical task (1). For solid samples, direct determination of trace distributions is still a challenge to analytical chemists. The basic requirements here (2) are microregion analysis and, ideally, depth profiling capabilities; high absolute and relative concentration sensitivities; minimum variation in sensitivity between elements; and freedom from matrix effects. All these require special techniques and devices. Two methods available for direct microanalysis of bulk solids are electron microprobe (3) and ion microprobe (4). Both these techniques offer excellent two-dimensional resolution and high sensitivity for direct solid analysis; however, the requirements of electrical conductivity of the specimens and high vacuum level in the sampling compartments pose difficulties in their applications, e.g., biological and medical analyses. Besides, electron microprobe is not sensitive enough for light elements ($Z < 11$) because of the Auger effect (5).

The advent of lasers has brought totally new possibilities to direct microanalysis of solids. Laser microprobe analyzer (LMA) came

into being only two years after the invention of the laser (6). The unique properties of lasers render LMA the following advantages:

1) High resolution microregion analysis. Lateral resolution as little as 1 micrometer can be achieved (7). Actually it is the required sensitivity rather than beam diffraction that limits the resolution. So LMA is an excellent tool for two-dimensional microregion analysis, such as analysis of mineral grains, metallurgical inclusions and material defects.

2) Compatibility with highly sensitive optical spectroscopic (8) and mass spectrometric (9) techniques. For atomic spectroscopy, relative sensitivity is in the ppm range and the absolute limit of detection is in the nanogram to picogram range, theoretical limit of detection can be even lower (10). For laser mass spectrometry, relative sensitivity is less than 1 ppm, and the absolute limit of detection can reach 10^{-15} to 10^{-19} gram range (11).

3) Freedom from selective vaporization (12, 13) and matrix effects (2) in comparison to other techniques like longer-lasting spark and arc excitation, or furnace atomic absorption. This freedom is especially present when Q-switched lasers are used, because of the high irradiance (e.g., 10^{9} W/cm^{2}) which is readily available.

4) Depth profiling capability with a resolution of better than 1 micrometer (14). This capability does not exist with electron microprobe.

5) Capability for simultaneous, multielemental analysis using spectrograph or polychromator, or mass spectrometer.

6) Capability to measure light elements ($Z < 11$) (15), which are difficult to analyze by electron microprobe since the Auger process dominates after the core electrons are ionized by an energetic electron beam (5).

7) Isotopic identification using laser microprobe mass spectrometry (16).

8) Versatility to handle the vaporized material to fit different needs. The plume can be analyzed either locally (17), or after transport to another location for observation or further excitation (18), or after condensation onto a collector for a second-stage excitation (19).

9) Unlimited types of solid samples including those electrically nonconductive or refractory materials, which are difficult to handle by other microprobe techniques.

10) Nondestructive nature due to the extremely minute amount of material actually removed (9), which is tolerable in most cases.

11) Ease of sample preparation. Direct, in-situ solid analysis is therefore possible; moreover, contamination from reagents, mortars and auxiliary electrodes can be avoided.

12) No need to keep the specimen under high vacuum level, unlike electron and ion microprobes; therefore, tissues and other biological objects can be studied, without the risk of sample dehydration or decomposition.

13) Lower cost in comparison to other microprobe techniques.

However, in spite of its strength, laser microprobe analysis suffers from several limitations:

1) Relatively poor accuracy; accordingly, use of standards of closely matched compositions is highly recommended (8).

2) Relatively poor signal reproducibility with a relative standard deviation in 10-30 % range (11, 20). This value can even reach 50 % for trace analysis in pellets of powered samples (21).

3) The damage on the sample, though minor, might not be tolelable in some situations.

4) Difficulty in realizing a continuous mode of sample introduction.

Because of these advantages and drawbacks, the laser microprobe analyzer (LMA) is complementary to other microprobe techniques.

Many optical spectroscopic techniques have been used to couple with laser microprobe for different analytical purposes. The first and the most straightforward detection scheme is to monitor locally the atomic emission in the sampling compartment (6). Auxiliary excitation is frequently needed to increase the emission intensity without increasing the crater size, especially for sample materials having low boiling points (22). The method most commonly used is spark discharge cross excitation (23), which results in higher sensitivity, narrower spectral lines and elimination of self-reversal, usually with the cost of poorer reproducibility (24). Other methods of auxiliary excitation developed so far include radio-frequency discharge (25), microwave plasma discharge (26), and direct current argon plasma (27). Laser-

induced breakdown spectroscopy (LIBS) has been applied to steel analysis, in which the atomic line emission is resolved from the background plasma continuum (28). Alternatively, the ablated material can be swept by an inert gas flow to an inductively coupled plasma spectrometer. One distinct advantage of atomic emission spectroscopy (AES) is the ease with which multichannel measurement may be realized using a photodiode array (18) or a polychromator (29). Use of a spectrograph usually requires multiple exposures.

To take advantage of the larger population of ground state atoms, atomic absorption spectroscopy (AAS) has been developed. The first application was realized by Mossotti, Laqua and Hagenah (30), who utilized a multiple-pass configuration to increase the lightpath. For those samples with low atomization efficiency, further heating by a graphite furnace proves useful (31). Laser-induced atomic fluorescence spectroscopy introduced by Measures and Kwong (32) has achieved high sensitivity without interference from chemical matrix effects (2). A two-stage method allows optimization of both sampling and excitation processes, since these are completely separated in space and time. At first, the laser-ablated material is collected onto the end surface of a graphite rod (33), or onto a transparent film (34) or a quartz plate (19). The condensate is then subjected to excitation and analysis. Adams and Tong demonstrated the ultrahigh sensitivities achieved by gamma and alpha spectrometry for radiative condensate, and neutron activation and mass spectrometry for nonradiative condensate (35). Mayo, Lucatorto and Luther showed the first successful hyphenation of

laser ablation and resonance ionization spectrometry for highly sensitive analysis of impurities in silicon samples (36).

Detection of the ionic species by mass spectrometry (9, 37) offers several unique capabilities including excellent sensitivity (11) and isotopic identification (16). In addition, by changing laser intensity to work in the laser desorption (LD) or laser ionization (LI) regime, analysis of the adsorbed species, the surface layer, and the interior can be realized using the same instrument (38). Structural elucidation is also possible from the fragment ions (39).

Since its first introduction in 1962 by Brech (6), LMA has well established itself as an appropriate tool for qualitative or semiquantitative solid microanalysis and has gained widespread use (11, 37). LMA itself can be used for rapid analysis of bulk materials. Owing to its excellent two-dimensional resolution, it has been applied successfully to the identification of inclusions and to analysis of elemental distributions in alloys (40), wood (41), ores (42), polymers (7), ceramics, and glass (43). It is worth noting that high spatial resolution is especially important in geological applications, because of the common occurrence of mineral intergrowths on a micron scale (44). Distributions of several inert isotopes in lunar samples have been analyzed in situ and their origins deduced (45). Fly ash has also been analyzed (46). When LMA is applied to the analysis of biological and medical materials, microanalysis can be achieved in vivo for a resected material. Various types of tissues have been analyzed for trace metallic contents (47, 48), even individual cells can be analyzed (49).

In-situ analysis of small deposits of organic or inorganic substances in a histological material has been realized (50). Because of its nondestructive nature, it is used to analyze archeological samples and forensic evidence (51). Its excellent depth resolution enables it to determine successfully the thickness of coating layers (52), and layer-by-layer impurity analysis of different solid samples (14). When laser irradiance is low to allow only desorption to occur, LMA can be used to test surface contamination for quality control problems (53).

To turn LMA from a qualitative and semiquantitative tool to a reliable quantitative technique, further insight into the laser sampling processes is always needed. From the theoretical point of view, laser-matter interaction is itself a significant subject which has attracted increasing attention and research enthusiasm. Unfortunately, laser sampling is a highly complicated and violent process involving vaporization, dissociation, excitation and ionization. Depending on ablation and surface conditions, not only can the material removed form atoms, and singly and multiply charged ions, but it also can form clusters (54), molecules, and even droplets and particles (55). This situation makes quantitation difficult, since the magnitude of the analytical signal is determined by the population of specific species. It is still a challenging task to fully elucidate all the highly transient processes taking place in such a small volume of laser plumes. Better understanding of these basic processes and mechanisms will benefit not only analytical chemists; but a vast community as well which is engaged in laser machining like drilling (56), welding (57) and

cutting (58), in material processing (59), and even in optical storage of digital information (60) and laser surgery (61). Finally, it is worth noting that the temperature and density of the laser-generated plasmas can be found elsewhere in the universe only in stellar interiors; therefore, it is not surprising that some research on laser-plumes is aimed at astrophysical simulation (62), controllable thermal nucleur fusion (63) and even military uses.

Overview of the Laser-Solid Interactions

Laser radiaions, being coherent, monochromatic and hardly divergent, can be focused onto a tiny spot on solid surfaces, delivering a very high power density for microsampling. Among the available laser types, Q-switched pulsed lasers compare favorably with free-running lasers from an analytical point of view (64). They typically attain a flux density in excess of 10^9 W/cm^2 in a single 10-100 nS giant pulse. Radiation above this irradiance level couples efficiently with solid surfaces due to the decrease in surface reflectivity. Target material undergoes more thorough vaporization and thus contributes to the analytical signal, instead of simply being removed as liquid droplets. More importantly, vaporization selectivity between different elements does not occur (12, 65); consequently, the chemical composition of the plume represents closely that of the sample under study. These two types of laser radiation result in quite different physical pictures.

The qualitative description below is limited only to plumes generated by Q-switched pulsed lasers.

For most metals, the energy threshold for vaporization is in the range of 10^6-10^8 W/cm^2 (66). At power level higher than 10^8 W/cm^2, surface reflectivities decrease abruptly (67), resulting in efficient solid-laser coupling despite the high original reflectivities (68). The radiation penetrates only to a short depth, typically less than the wavelength. In this surface layer, the electrons in the conduction band absorb the laser radiation by internal photoeffect (69) and transit to higher energy states. In a good conductor, the mean free time between electron collisions is of the order of 10^{-14} to 10^{-13} second, so the energy absorbed by the electrons is distributed and passes to the lattice. Within a very short time, e.g., less than 1 nS at 10^9 W/cm^2, critical temperature can be reached in a thin surface layer (70). This critical temperature can be much higher than the boiling point under ordinary conditions because of the pressure exerted by the extremely rapid vaporization (71). For transparent dielectrics under sufficiently high laser flux, the laser energy absorption results from several mechanisms such as multiphoton ionization and non-linear effects, in particular, an avalanche-like multiplication of electrons (72) is believed to be the dominant mechanism. This also leads to a high surface temperature and subsequent rapid vaporization.

The net effect of this interaction is a thin layer of partially ionized, relatively cold and dilute plasma, known as primary plasma, near the target surface. The incoming laser radiation is then absorbed

in this primary plasma by inverse bremsstrahlung (free-free electron-photon interaction) (73), increasing the electron temperature, which in turn leads to further ionization. The heating of plasma itself is a result of electron-ion collisions. The plasma temperature approaches the electron temperature only under a relatively low irradiance with a sufficiently long pulse duration (74). The increase in electron density results in more efficient absorption and further ionization. Finally, the electron density approaches a critical density in a layer of the plasma called the deflagration zone (75). In this zone, the plasma frequency matches the radiation frequency, and the plasma becomes reflective to the incoming radiation. The absorption coefficient of the plasma layer immediately in front of this zone becomes very high. As a result, the target surface can be temporarily shielded from the radiation (76), and the plasma is heated to a high temperature.

The radiation from the plume is black body radiation at the early heating stage, which is usually negligible. Near the end of the giant laser pulse, the blow-off material becomes so hot, around 2 eV at 10^8 W/cm^2 to 100 eV at 10^{12} W/cm^2 (77), that thermal radiation starts (78). Blemsstrahlung dominates the continuous radiation, with some contribution from electron-ion recombinations. Those characteristic line emissions from the excited atoms and ions superimpose on the continuous background. Much energy is in the hard UV and X-ray range, which can play an important role in ionizing the neutral species in the plume (79). The portion of radiation reaching the surface leads to further vaporization (80). The degree of ionization of the ablated

material, governed by the Saha-Langmuir equation, is highly dependent on the power density of the vaporization beam. Below 10^8 W/cm^2, the degree of ionization is very low, of the order of magnitude of 10^{-5}; while at 5 x 10^9 W/cm^2, it can approach 100 % (37).

At the same time, a pressure wave is initiated and propagates into the interior of the sample, owing to two mechanisms. The first is the recoil of the removed material, which leaves the surface at high speed (71). The second is the thermal expansion of the heated layer, which exerts a pressure on its adjacent layer and hence generates a compressive shock wave travelling through the solid target (80). It is therefore independent of the material removed from the surface.

Driven by the high pressure gradient, the plume expands into low pressure background gas or vacuum. The thermal energy then converts into kinetic energy of the orderly expansion. The velocity of expansion can be very high, depending on the incident laser power density and the atomic mass number of the target material (81). Ion-electron recombination (82) and fragmentation of bigger clusters (83) also occur during the expansion. As a result of expansion and recombination, the electron density decreases rapidly, so that the plasma cloud becomes transparent to the incoming beam again and cools down rapidly.

A crater with an annular rim is formed on the sample surface, as a result of vaporization, sublimation, melting-flushing, and solidification (84). Sputtered debris can be seen deposited outside this crater.

Introduction to Diagnostic Techniques for Laser-Generated Plumes

For experimental studies of laser-solid interactions, especially in the diagnostics of laser-generated plumes, several difficulties are encountered. These are small physical dimensions (~1 mm); high densities ($\sim 10^{20}$ cm^{-3}); high expansion velocities (up tp 200 km/sec) and, in particular, the fact that due to highly transient nature of the event, the plasma is in neither collisional nor radiative equilibrium. Interpretation of the observation, therefore, must be done with caution.

Various experimental approaches have been undertaken to investigate the plumes generated from solid targets under pulsed laser radiation. High speed photography is a straightforward tool to measure the plasma expansion rate and the temporal evolution of the plasma cloud as a whole (85). Both time-integrated and time-resolved studies can be performed. Time resolution of 5-10 nS can be obtained, either with streak cameras or with frame cameras. Time-of-flight measurements (86, 87), or electrostatic analysis (88), or retarding potentials (89, 90) are techniques to measure the final kinetic energy of ions; however, owing to the time delay involved, information in the early stage of plasma development is lost, and real-time information cannot be obtained by these methods. Similar restrictions apply to the electrostatic and mass spectrometric methods.

By optical interferometry (91, 92), optical refractivity of the plume can be measured in real time. If the contribution from the electrons dominates in the refractive index of the plasma, then electron density can be measured. This, in combination with the optical density of the plume, allows the calculation of electron temperature (93). In some cases the contributions from atoms and ions cannot be ignored. Where this occurs, separation of the electron and mass components is possible from interferometric measurements made at two wavelengths (94). Microwave interferometric measurement, based on the same principle, can follow the decay of electron density over a longer period of time than its optical counterpart (95). When the electron density reaches a certain critical level, the plasma boundry becomes reflective to the incoming radiation. This phenomenon can be used to measure the expansion speed of the plasma front (96).

One of the most powerful and fruitful techniques to study the laser plume is the optical spectroscopy. Atomic and molecular absorption spectroscopy has been used by Steenhoek and Yeung (97) to provide concentration mapping of ground state species. Since emission lines from highly ionized species, especially their resonance series, tend to be in the vacuum ultraviolet to X-ray spectral regions, spectroscopic measurements in these regions (98) yield information about the populations and ionization states of these multiply charged ions and their temporal evolution. The Doppler broadening of emission lines can be used to determine the expansion speed of the emitting species (99). At high electron densities, the Stark effect predominates the line

broadening; as a result, from the experimentally observed line profile, electron density can be calculated (100). A variety of methods is available for temperature estimation, e.g., relative intensity measurement of various spectral lines (101).

Light scattering is another useful technique capable of offering information about density distribution within the plume. Izawa et al. use this technique to record both electron and neutral atom density profiles within a carbon plume (102). The scattered light arises from Thomson scattering from the plasma at the early stage, while that from Rayleigh scattering from neutral species arises at a longer time scale. For relatively large particles, mie scattering is the tool of choice to study the particulates formed in laser plumes. It has been applied by Huie and Yeung (55) to measure the concentrations, and by Kimbrell and Yeung (103) to measure the sizes of the particulates generated from different materials

Mass spectrometry, due to its inherent strength, is a good tool to investigate the formation of atoms, ions, and clusters; as well as their ionization stages, relative abundance, and energy spectra (104). Finally the recombination and disintegration processes can be deduced. If local thermal equilibrium is valid within the plume, then the Saha equation can be used to determine the temperature from these measurements.

From the standpoint of optical spectroscopy, characterization of neutral species is of exclusive importance. Unfortunately, available techniques for neutrals are relatively limited in comparison to those

for charged particles. Besides, to fully understand the transient processes within the laser plumes, both temporal and spatial information is essential. Special consideration must be made of the design of experimentation to achieve these goals.

A new universal density probe, capable of providing well-resolved spatial and temporal information, is described in Section I (105). The probe is based on the refractive index gradient which is developed within a laser-generated plume, as a result of the density distribution. It is suitable for monitoring the dynamics of those neutral and nonemitting species, as well as charged and emitting ones, in highly transient events like laser vaporization. Detection limit of 1 ng has been achieved.

In the remaining part of this thesis, a new normalization method is suggested for laser microsampling (106). It is based on the correlation of acoustic and spectroscopic signals associated with laser-generated plumes. To effectively couple the acoustic signal to the microphone sensor, an inert gas at a selected pressure was introduced into the sample cell. It has been found that fairly good linear correlation is maintained between these two signals, under widely varied experiment conditions such as laser power, focusing, surface treatment; and, to a limited extent, chemical composition. It is, therefore, possible to use the photoacoustic signal as an internal standard for quantitation of laser sampling. This would improve the reproducibility of laser microprobe analysis.

SECTION I

A SPATIAL AND TEMPORAL DENSITY PROBE FOR LASER-GENERATED PLUMES BASED ON BEAM DEFLECTION

INTRODUCTION

Because of their unique properties, lasers have become indispensable tools today. Many of their applications are based on laser-solid interactions; e.g., laser machining, material processing and even digital data storage and astrophysical simulation, not to mention controllable thermal nuclear fusion and military uses. For analytical chemists, lasers have been widely used as intense, highly monochromatic, collimated and coherent light sources for various spectroscopic techniques like absorption, fluorescence, and Raman spectroscopy (1). Another important analytical use is the laser microprobe analyzer (LMA), in which the laser radiation is focused onto a microregion on the surface of a solid sample. A tiny amount of material is vaporized from the irradiated spot and then analyzed. Because of its outstanding two-dimensional resolution and depth profiling capabilities, as well as its compatibility with highly sensitive optical spectroscopy (2, 3) and mass spectrometry (4, 5), LMA has been utilized successfully in direct microsampling of solids of unlimited types.

This success, as well as the problems associated with laser applications, has stimulated further investigation into basic laser-solid interaction processes. This situation is similar to the earlier studies of discharge and nebulization processes, and all kinds of sample introduction devices, which has in part led to the current success in

atomic emission and absorption spectroscopy using arcs, sparks, flames, plasmas and furnaces.

Despite the strength that lasers have shown in microprobe analysis, however, LMA has its own limitations; namely, relatively poor accuracy and repoducibility (6). This is partially due to the pulse-to-pulse fluctuation of laser output power and variations in other experimental parameters, and partially due to physical and chemical matrix effects. Consequently, the laser microprobe analyzer remains only a qualitative or semiquantitative tool (7, 8) since its first introduction a quarter of century ago (9). Better understanding of laser-solid interactions is definitely needed for optimizing sampling conditions, fully utilizing the ablated material, improving its accuracy and repoducibility, and hopefully developing LMA into a reliable analytical technique.

From the standpoint of analytical chemistry, more interest is focused on the chemical forms and the quantities of ablated material, their excitation and ionization states, their spatial distributions, and their temporal development. Among various diagnostic methods, electrostatic techniques, by using electrostatic double probes (10) or charge collectors (11), or based on time-of-flight measurement (12), can provide information about the densities of charged particles, their expansion velocity, and angular distribution. These methods, however, by their very nature, are only useful for probing charged particles. The spatial resolution is limited by the physical sizes of the electrodes used. Besides, to avoid spurious perturbations in the plume,

the electrostatic probe cannot be placed too close to the plume center; this excludes the ability to gain any useful information close to the central region of the plume, where most of the important processes take place. Moreover, due to the time required for the particles to travel from the irradiated spot to the collector electrodes, information about the early stage of plume development is lost and real-time imformation is impossible. Mass spectrometry is another powerful diagnostic tool for laser plumes. Charge-to-mass ratios of particles can be measured using a quadrapole spectrometer (13). Momenta of ions can be measured using sector spectrometer, time-of-flight spectrometer (14), or electrostatic analysis (15). For similar reasons, however, it suffers from low spatial resolution, real-time measurement is also impossible.

Other methods, especially those based on sensing some forms of electromagnetic radiation, are being sought and developed persistently. Among the plume parameters, expansion velocity and density of individual species are of considerable importance. The former is usually obtained using high speed photography (16), time-of-flight measurement (17), and Doppler shift (18). A basic requirement here is that the species must either emit or absorb light to become observable. Density mapping of atoms and molucules have been obtained using absorption spectroscopy (19, 20). Electron density usually can be obtained from interferometry (21), or from Stark broadening of the emission lines (18). By interferometry, the overall refractivity is measured, which might include contributions from both electrons and mass (atoms and ions). To separate these conponents, two probe wavelengths can be used (22). In

order to get a time and spatially resolved interferogram, the probe laser beam can be split into several beams before entering a Mach-Zehnder interferometer cavity (23). These beams can then be used to probe different positions of the plume to gain a more complete picture. Excellent temporal resolution can be achieved. But the ultimate spatial resolution is still limited by the physical size of the probe laser beam throughout the interferometer cavity.

In the past few years, two distinct types of spatial probes have been developed. Firstly, a continuous laser, properly gated by an electronic shutter, is beam-expanded to cover the entire cross-section of interest. The spatially varying signal is then registered on a vidicon camera (19). Since the camera is an integrating device, the temporal resolution is provided by the electronic shutter. Secondly, the continuous laser can be directed by an acoustooptical beam deflector to scan through the spatial region of interest at high sweep rates. The laser beam is focused at the probe region to provide spatial resolution but is subsequently imaged onto a single photodiode (20). Spatial information is thus transformed into temporal information at the photodiode output, and can then be digitized and analyzed using a waveform analyzer. The transient event is essentially "frozen" in time at each sweep. Consecutive sweeping can then provide temporal information about the development of the transient event. These two types of probes have been used to map atomic and molecular concentrations (19, 20), translational temperatures (24), vibrational temperatures (25), particle concentrations (26) and sizes (27).

In cases where the species vaporized by the laser does not absorb or emit at convenient wavelengths, or the concentration is too low to provide measurable scattering signal, then the spectroscopic probes based on absorption and scattering will not work. A more sensitive and universal probe is then needed for these events.

In this section, a density detector is described which is capable of providing spatial and temporal information for those transient events. It is based on laser beam deflection (BD) owing to the refractive index gradient inside the plumes, which is a consequence of the density gradient developed during the plume expansion. The resulting beam deflection signal can then be monitored by a position sensing detector in far field. Since the probe beam can be focused down to a small beam waist within the laser plume, generating a BD signal in a single pass, both spatial and temporal resolutions are very high, and the density information can be obtained in real time.

This is analogous to the photothermal deflection (or so-called "mirage effect") (28, 29) previously used in developing the concentration gradient detector for electrochemistry (30), for flowing gas stream (31) and for liquid chromatography (32). It is important to distinguish the two, since in laser plume diagnostics using beam deflection, time is not sufficient to establish a thermal gradient (too few collisions), even though the ejected materials themselves might be high in temperature. The vacuum is the background here so the flow disturbances and thermal fluctuation do not contribute to the noise.

THEORY

The refractive index of a gaseous medium with i components is given by the Gradstone-Dale formula (33):

$$n - 1 = \sum_i k_i N_i \qquad (1)$$

where n is the refractive index of the mixture, N_i is the number density of the i-th component and k_i is the specific refractivity of the i-th component. In the case of laser-produced plumes, neutral atoms, ions, electrons and small clusters all have their respective contributions to the overall refractivity. This will be further discussed below.

The propagation of a Gaussian beam through a medium with a spatially varying index of refraction is described by the paraxial equation (34):

$$\frac{d}{ds}\left(n_o \frac{dr_o}{ds} \right) = \nabla n(r,t) \qquad (2)$$

where s is the light path, r_o is the perpendicular displacement of the beam from its original direction, n_o is the uniform index of refraction, and $\nabla n(r,t)$ is the gradient of the index of refraction perpendicular to the light path.

When applying the beam deflection technique in diagnostics of a laser-generated plume, one has to deal with the fact that the event is a

highly violent process with very short time duration. However, under certain conditions the dynamics of the plume can be simplified by the following assumptions:

1) Instantaneous plume generation. This is a fairly good approximation when the duration of the giant laser pulse used (in this case 25 nS) is much shorter than the time of plume-probe beam interception.

2) Complete vaporization without generation of clusters or droplets big enough to attenuate the probe beam (35). This can be accomplished when a Q-switched pulsed laser of appropriate wavelength is used for sampling, and the radiation density is controlled at a moderate level. These tend to lead to efficient vaporization without generating a large amount of molten meterial (2). This was confirmed in this work by microscopic observation of the laser craters.

3) The wavelength of the probe laser is selected in such a way that the absorption and scattering by the plume can be neglected. This can be achieved when the wavelength of the probe laser is far away from the resonance lines of the plume species. Since we are dealing with collections of atoms using 632.8 nm HeNe wavelength, this can be satisfied fairly well. When monitoring the deflected probe beam in far field, scattering can usually be neglected because of its very small cross section.

4) The atoms generated have uniform vertical velocity v leaving the surface. It has been found, though, that the mean squared ion velocity increases proportionally to the square root of the laser pulse

peak intensity for the lower atomic-weight materials (36). But if the pulsed beam is well focused onto a small enough area, so that the cross-sectional power density variations are effectively averaged out by rapid heat transfer, then this assumption is valid.

5) Assuming that the atoms ejected are only subject to internal pressure, then their radial expansion will be isotropic. During the relatively short time of observation, both expansion and vertical drift velocities can be approximated fairly well by constants. Therefore, a spherical plume results, which can be described by its radium R and angle of expansion 2α. This isotropic plume expansion has been observed using a high speed camera (37). Many researchers, on the other hand, have reported conical plume expansion, e.g., in Ref. 38. These two pictures can be considered equivalent for the same physical process, since simultaneous linear radial expansion and linear vertical drift result in a conical envelop.

6) Finally the density profile of the plume can be described by a radially linear function

$$N^r = \left(1 - \frac{r}{R} \right) N^o \qquad (0 \leq r \leq R) \tag{3a}$$

$$N^r = 0 \qquad (r > R) \tag{3b}$$

where N^r is the number density inside the plume at a distance r away from the center of the plume, N^o is the number density at the center of the plume. This radially linear density profile has been proposed by

other workers (39). The topic of plume density distribution deserves more discussion later.

Under these conditions, the dynamics of the plume can then be depicted in Figure 1, where h is the probing height, vt is the distance of the moving plume center above the sample surface at time t, and L is the light path inside the plume. To carry out the calculation, Eqn. (1) can be rewritten as

$$\frac{\partial \Phi}{\partial x} = \frac{1}{n} \frac{\partial n}{\partial y} \tag{4}$$

and the angle of deflection $\Delta\Phi$ can be obtained by integrating Eqn. (4) over the light path L within the plume:

$$\Delta\Phi = \int_0^L \frac{1}{n} \frac{\partial n}{\partial y} \, dx \tag{5}$$

Considering the fact that all gaseous media have values of n very close to unity, which is especially true when the amount of material ablated by the laser pulse is little, then 1/n can be approximated by constant 1 and removed out of the integral. This leads to the following result:

$$\Delta\Phi = \frac{6N_o k (h - vt)}{\pi (vt \sin \alpha)^4} \ln \left\{ \tan\left(\frac{1}{2} \arcsin\left(\frac{h - vt}{vt \sin\alpha}\right)\right)\right\} \tag{6}$$

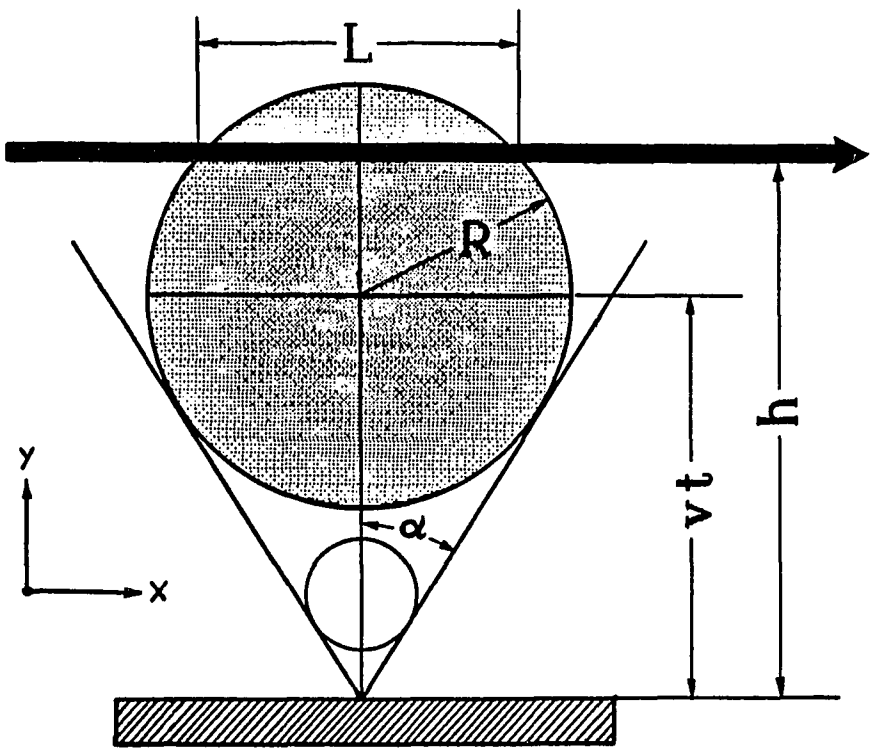

Figure 1. Simplified picture of plume-probe beam interception: h, probing height; R, radius of laser-generated plume; l, light path inside the plume; vt, distance of plume center above the sample surface at time t; 2α, angle of expansion

where N_o is the total number of atoms blown off in each laser pulse. All the parameters in this expression can be obtained experimentally, so the angle of deflection can be calculated and then compared to the experimental results. The beam deflection signals expected from the different stages of laser-probe beam interception are depicted in Figure 2. Detailed derivation of Eqn. 6 is given in the Appendix at the end of this thesis.

Figure 2. Beam deflection signals at different stages of plume-probe beam interception

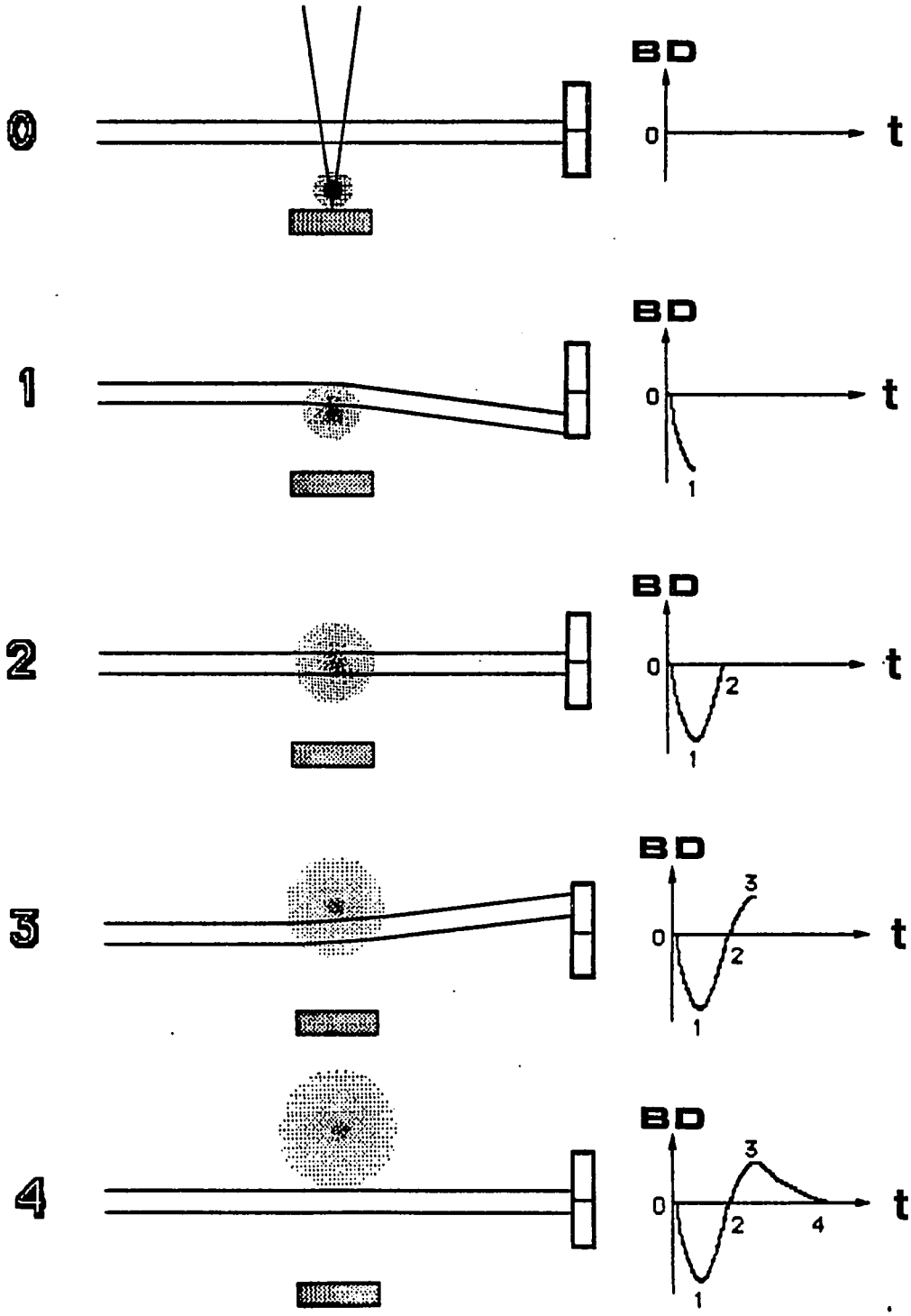
0
BD
0
t
1
BD
0
t
1
2
BD
0
t
2
1
3
BD
0
t
3
2
1
4
BD
0
t
3
2
4
1

EXPERIMENTAL SECTION

A block diagram of the experimental setup used in this work is shown in Figure 3. The solid sample used was a 1/8" x 1/4" x 0.5 mm piece of p-type, single-crystal silicon wafer with resistivity 5.5-9.3 ohm-cm (SEH America, Vancouver, WA). The sample piece was mounted on the end of a 1/4" glass rod inside a sample cell using five-minute epoxy, with a polished 111 surface facing the laser. The surface of the sample was cleaned with acetone before use without further treatment. To enable independent movements of the sample in all directions, the sample cell was mounted sideways on a homemade tilt/3D translational micrometer stage. The cell was connected to a vacuum chamber. A two-stage glass diffusion pump, capable of achieving 10^{-5} torr, was used.

A Model HyperEX 460 excimer laser (Lumonics, Ottawa, Canada) operated at 308 nm XeCl transition was used as the sampling laser. UV radiation was used because of its efficient coupling with solid samples (40). The output energy of the laser pulse was rated at 31 mJ/pulse and the duration was 25 nS. Typically the sampling rate was under 2 Hertz, so that sampling would not be affected by the previous event. The energy used for sampling was adjusted by varying the diameter of the aperture A and the voltage of the power supply. This energy was monitored by using an energy ratiometer (Laser Precision, Utica, NY, Model Rj-7200) with an energy probe (Laser Precision, Utica, NY, Model RjP 734). The pulse-to-pulse power fluctuation was measured with a

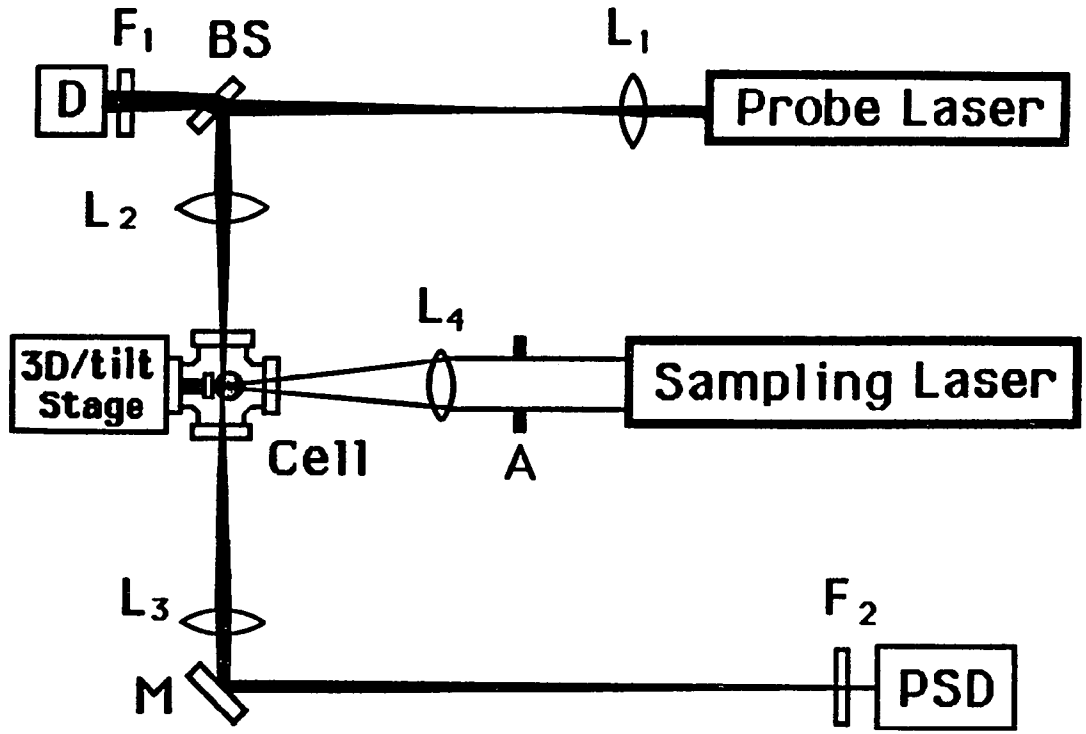

Figure 3. Experimental arrangement for measurement of beam deflection caused by laser-generated plume: A, aperture; BS, 50 % beam splitter; D, reference beam detector; F1, F2, 632.8 nm line filters; L1, L2, L3, plano-convex glass lenses; L4, UV plano-convex quartz lens; M, mirror; PSD, position sensing detector

relative standard deviation (RSD) of ± 1.4 %. The pulsed UV beam was focused onto the surface of a solid sample using a planoconvex UV-grade quartz lens L_4 with a focal length of 7.5 cm (Oriel, Stratford, CT). Normal incidence was assumed in this work. Typical power density used was below 10^9 W/cm^2.

A HeNe laser (Spectra-Physics, Mountain View, CA, Model 248) operated at 632.8 nm was used as the probe laser. Double-beam configuration was assumed in this work to compensate the output fluctuation of the probe laser. The transmitted beam through a 50 % beam splitter (BS) was used as a reference beam and monitored using a photomultiplier tube (Hamamatsu, Bridgewater, NJ, Model R928). To ensure high spatial resolution as well as high sensitivity, a highly compact probe beam waist was always desirable. This was achieved by first expanding the beam and then refocusing it. Two planoconvex lenses L_1 (f 4.6 cm) and L_2 (f 25 cm) separated by 170 cm was used for this purpose. The beam waist was located 0.5 mm in front of the irradiated spot. Careful alignment of two laser beams proved very essential to getting high sensitivity. This was done by first creating a crater on a piece of microscope slide using the pulsed laser, and then aligning the HeNe beam with this crater with the help of a magnifying glass. Another planoconvex lens L_3 with focal length 15 cm (Oriel, Stratford, CT) was used to focus the beam onto the position sensing detector (PSD). By this arrangement, any deviation of the spot shape of the probe beam from circular Gaussian profile will have minimal effect. As pointed out by

Mandelis and Royce, this can develop after the beam has emerged from a inhomogeneous gradient of refractive index (41).

Two types of PSD's were used throughout this study. One was a UDT bicell photodiode detector (United Detector Technology, Hawthorn, CA, Model PIN-SPOT 2D) with 6.45 mm^2 sensing area. The other was a knife edge/photomultiplier arrangement. The latter is much more sensitive than the former because the high output current makes the amplifier noise negligible. A micrometer translational stage was used to mount the bicell detector or the knife edge to make possible fine alignment. Typically the position of the knife edge was such that 50 % intensity was registered by the photomultiplier tube. Thus, the intense HeNe beam center was located right on the knife edge position to ensure maximum sensitivity. Both outputs from the reference beam and deflected beam were sent to a Tektronix Model 7704A oscilloscope (Tektronix, Beaverton, OR) with a Model 7A22 differential amplifier module. AC (alternative current) coupling is used in all signal channels to provide a stable base line, minimizing the effects of long-term noises. A Tektronix oscilloscope camera was used to take hard copies of the screen display.

The stray light was kept at a minimum level. Pinholes and 632.8-nm line filters (Corion, Holliston, MA, Model 30-6328-1) were used in front of both detectors. To reduce the noise caused by mechanical vibrations, all optical components were mounted as rigidly as possible on a 4' x 6' x 2" optical table (Newport, Fountain Valley, CA, Model NRC XS-46), which was padded with a sheet of 1/8"-thick rubber. All the mechanical pumps used in the same room were padded with 1" to 2" thick

foam plastic sheets to absorb vibrations. The bulky excimer laser was mounted on another bench, and its beam was directed to the cell using a mirror (Newport, Fountain Valley, CA, 10QM20EM.15). The air turbulence was another important source of interference; therefore, to reject its influence, the whole probe beam lightpath was shielded with 1" glass tubing. Both ends of the tubing were sealed with pinholes with central holes slightly larger than the size of the probe beam. Finally, those pieces of equipment generating heat and hot air flow, e.g., power supplies and oscilloscope, were allocated far away from the optical table. To ensure stable operation, the HeNe laser used was selected among several according to their AC/DC level, and it was warmed up for long enough time period before data were taken.

The average amount of material removed by each laser shot was measured by weight difference before and after laser ablation. To reduce weighing error, the sample was exposed to more than 10000 laser pulses over different spots, with 170 to 180 exposures on each spot. The calculation was done on an Apple Macintosh 512KE computer with 128K ROM and 512k RAM on board, the program was written in Microsoft BASIC version 2.0. Photomicrographs were obtained from a metallurgical microscope (Olympus, Lake Success, New York, Model BHM) with a PM-10AD camera. By focusing first at the bottom of the crater and then at the sample surface, the depth of the crater was estimated from the reading difference of a calibrated dial.

RESULTS AND DISCUSSION

Interpretation of Experimental Results

Using the experimental arrangement shown in Figure 3, beam deflection (BD) signals similar to those shown in Figure 2 were indeed observed. For a surface spot under a series of superimposed shots, both the peak shape and the magnitude of the deflection signal change considerably with the number of exposures. The first few shots give very weak signals with a single negative peak. Then a positive peak appears following the negative peak. Both these peaks gradually increase in magnitude and become more symetrical with respect to the point of zero crossing. These trends continue until approximately 120 shots. Then the signal magnitude starts to decrease. After about 300 shots, the BD signal decayed to zero. It is obvious that a theoretical model is needed to explain these results, both qualitatively and quantitatively.

It was found that under common experimental conditions, the bicell photodiode detector gave an approximately linear response; therefore, comparison of experimental results with the theoretical model was done on the bicell signals. To apply Eqn. (6), N_o, k, h, v, and α must be evaluated. The total number of atoms per shot, N_o, can be obtained from the weight difference per shot, or by means of microphotography. The specific refractivity of silicon, k, can be calculated from the

refractive index of bulk silicon (42-44). The probing height, h, can be easily measured from the readings of micrometer on the 3D stage. The vertical velocity, v, can be calculated from the peak position change at different probing heights, as is shown in Figure 4. Explicitly, the time taken to reach zero crossing (position 2 in Figure 2) is simply h/vt. However, the expansion angle, 2α, can only be obtained experimentally for those emitting species, e.g., in a copper plume. For nonemitting species, this value must be fitted. The calculated curves at 2α = 100 degrees to 30 degrees at 10 degree intervals are shown in Figure 5. It can be seen that when the expansion angle decreases, the BD signal always narrows, corresponding to a shorter time of interception. The change of magnitude follows a more complicated pattern: the signal from the top hemisphere decreases first, reaches a minimum at around 2α = 80 degrees, then increases again. The signal from the bottom hemisphere, on the contrary, always increases. When the angle reaches 45 degrees, its magnitude increases sharply.

The curve fitting for the 80th, 120th and 160th laser shots are shown in Figure 6. From these the whole picture of successive laser vaporization events becomes clear: when the laser irradiance was low, the first several shots generated little damage on the perfect surface. This was parallel to other observations, e.g., in Ref. 45. Then evaporation become more efficient because the surface was roughened. At the early free-expansion stage, the expansion angle is large. When the probe beam is intercepted by the bottom hemisphere of the plume, the vertical velocity of the plume leaving the target is partially

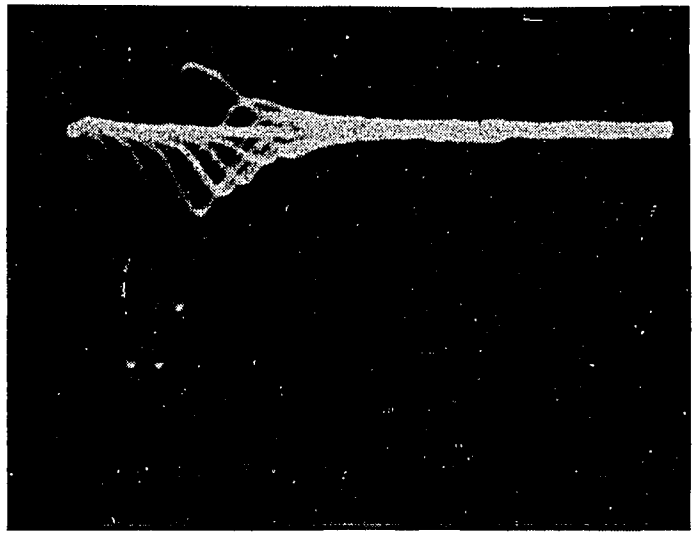

Figure 4. Beam deflection signals obtained at different probing heights. Curves 1 to 9 (from left to right) correspond to probing heights of .020", .025", .030", .035", .040", .045", .050", .055" and .060", respectively. Sample, silicon wafer; sampling laser, Hyper EX460 excimer laser at wavelength 308 nm, duration 25 ns and energy 8.3 mJ/pulse; X scale, 2 μs/division; Y scale, 200 μV/division; position sensing detector, UDT PIN-SPOT 2D bicell photodiode

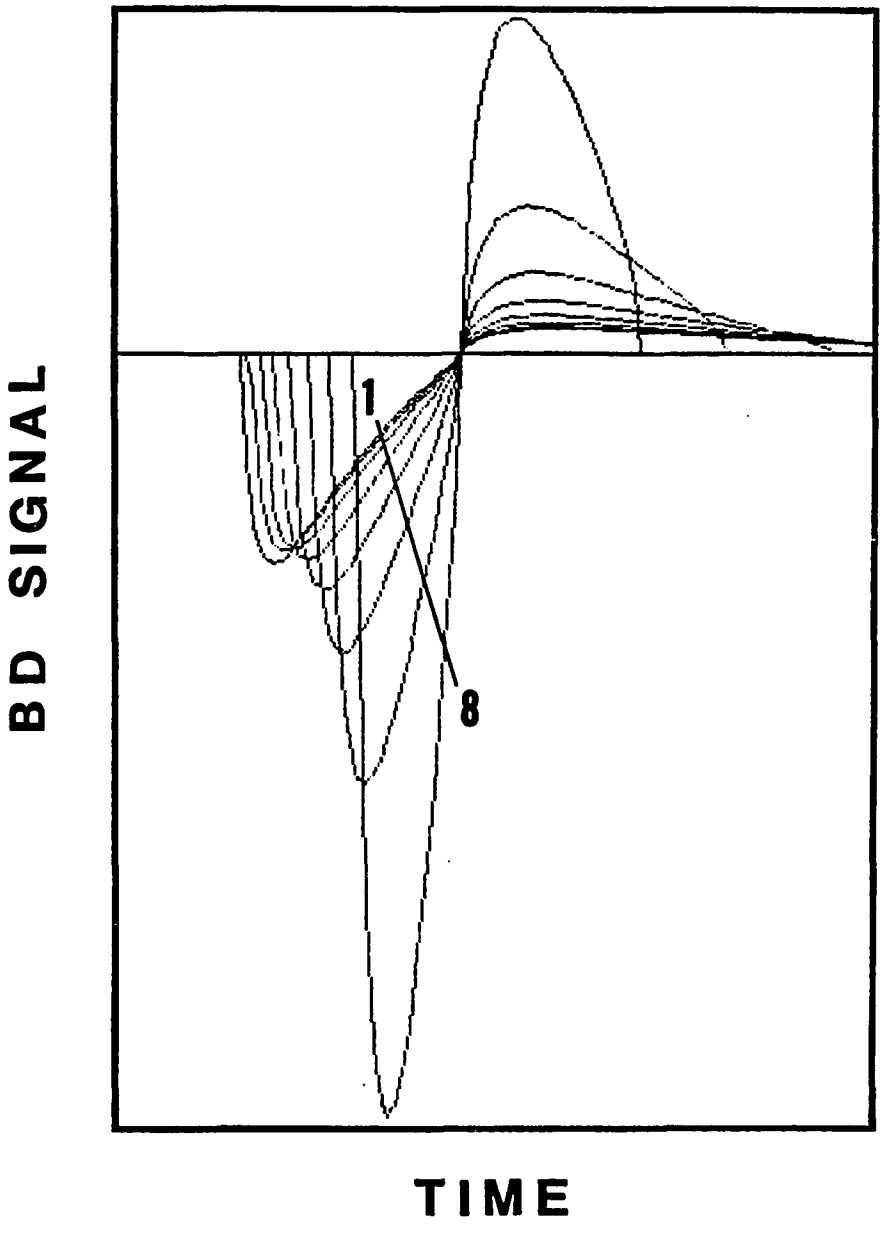

Figure 5. Calculated beam deflection signals using Equation 6. Probing height, h, 0.05 cm; vertical velocity of the plume center, v, 13900 cm/s; angle of expansion, 2α, 100^{o} (curve 1) to 30^{o} (curve 8) at 10^{o} intervals

Figure 6. Curve fitting for BD signals from the 80th, 120th, and 160th laser exposures on the same spot of silicon surface. Column A, experimental BD signals from a bicell detector on the indicated silicon plumes under vacuum; column B, calculated BD curves from those experimental parameters shown in Figure 5 except the angle of expansion 2α, which is set at 105°, 45°, and 30° for the corresponding exposures

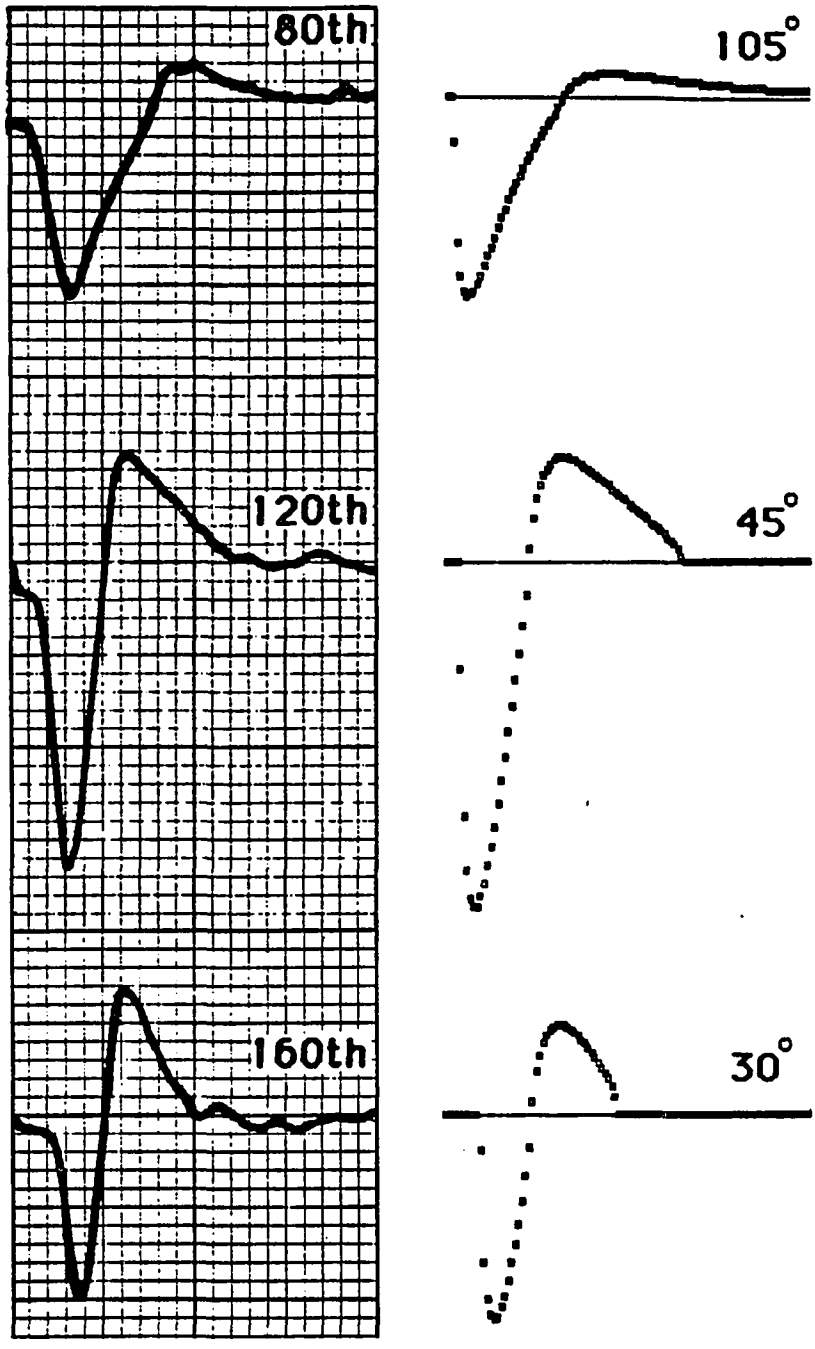
80th
120th
160th
105°
45°
30°
(A)
(B)

compensated by the rapid radial expansion. The resulting positive peak, therefore, is flat with relatively long time duration, which can be mistaken easily as missing. This is what happened at the first several laser exposures. With more material removes as a combined result of vaporization and melt flush (46), the crater becomes deeper and an annual rim builds up around the crater. These processes cause the expansion to become more confined and hence more directional. This corresponds to a small expansion angle, so the positive and negative peaks become more symmetrical with respect to the point of zero crossing. At about the 120th shot, maximum deflection is observed. After that, the crater becomes even deeper that the focusing of the vaporization laser changes considerably and hence the power density decreases. In addition to the depth development, the rim continues to build up; as a consequence, it becomes more difficult for the atoms to escape. This leads to a decrease in the signal magnitude.

It is found that laser blow-off is usually confined in a cone centered about the target normal (38, 47); however, under certain conditions, highly directional expansion has been observed (48). Therefore, the curve fitting of the BD signal suggests a method for evaluation of expansion angle even for those nonemitting species. These results imply the correlation between the plume expansion and the crater geometry. It is interesting to note that a similar relationship has been observed by other researchers using a totally different approach (49). By collecting the erosion products on a glass plate in front of the target, it was found that the ejected material was distributed over

a solid angle whose generatrices were more or less a continuation of the crater wall. The definite advantages of BD measurement over the above mechanical method are that, since no collector is used, the vaporization event is totally unperturbed by the observation; and more importantly, the sensitivity of the BD measurement allows observation in a single laser shot. In contrast, multiple exposures are required to accumulate sufficient erosion material on the collector to reach any meaningful conclusion. The expansion angle might change during this collection process.

The BD signal amplitude is directly proportional to the total amount of evaporated material in each laser shot. For the 120th-shot signal, the deflection angle of 0.047 radian was calculated from the interception of the laser and the plume at the bottom hemisphere, which is in reasonably good agreement with the experimental result, 0.058 radian. This indicates that whenever the angle of expansion is known by means of curve-fitting, the amount of evaporated material can be calculated from the observed BD signal.

Although a uniform radial density profile has been assumed theoretically (50), and observed interferometrically (21), for laser generated plumes; the dynamics of free plume expansion suggests the development of a positive density gradient towards the plume center (51). Furthermore, constant radial density implies sharp density rise and drop in the plume boundaries. Then two BD signal jumps should be observed when the moving plume is just entering and just leaving the probe beam. However, experimentally when the beam deflection starts to

occur during a series of superimposed exposures, it seems that the BD signal consists of a single negative peak. The occurrence of a negative peak here could be explained equally well by the fact that the plume was very compact at the early expansion stage. The seemingly missing of the positive peak can be explained as is stated above. The curve fitting strongly implies that BD peaks occur somewhere inside the plume rather than at the plume boundaries, and a linear density profile is closer to reality than a uniform density distribution. Because of its relatively limited spatial resolution, interferometry cannot yield spatial information as reliable as beam deflection measurement.

Physically it is the pressure gradient within the plume that drives the thermal expansion. A radially linear density profile thus is a more reasonable approximation than the uniform profile. The same density gradient has been employed by other workers (39), which gives the major features of the plasma formation and subsequent expansion. However, the choice of a linear density function is somewhat arbitrary, and this approximation is doubtless not exact. A more exact model requires an even steeper density gradient approaching the plume center. Examples are the Gaussian profile (52), the reciprocal square root profile (53), the exponential profile (54), and those models with even more complicated functions (55). The beam deflection technique, because of its high spatial and temporal resolution, provides a new experimental approach to test these density models.

We also note that the time scale here is much longer than that in Ref 25; thus, our results are consistent with subsequent expansion of

the plume. In this work higher vertical velocity v is also observed when the irradiation power density is high, as indicated by the shorter time delay and the shorter overall peak duration. This is also consistent with observations using other techniques (36).

With a switch from the bicell detector to knife-edge/PMT arrangement, much higher sensitivity was achieved. This is because the high gain of the photomultiplier tube allows measurements away from the region dominated by instrumental electronic noise. Shown in Figure 7 is the phototube signal from a plume produced by a 4.4-mJ ultraviolet laser pulse on a silicon sample. At this energy level, the amount of material removed in each laser shot was only 12 ng. The signal-to-noise ratio (S/N) obtained here was about 30; hence, with S/N = 2.5, nanogram detectability was achieved for a single-shot measurement.

Our conclusions about the expansion angle and the derivation of N_o (material vaporized per shot) can be confirmed by photomicroscopy. This is shown in Figure 8 for a crater generated by 177 laser shots at 4.4 mJ/pulse. The oval-shaped hole resembles the shape of the pulsed laser beam before focusing. The major and minor axes of the hole measure 130 and 60 micrometers respectively. The depth, as determined by focusing at different planes from the surface and cleaving the piece of silicon, of 157 micrometer implies that a total of 2.5 microgram of silicon was removed from the hole. This corresponds to an amount of 14.3 ng removed in each pulse. Not all material leaves as vapor. When the irradiated spots are observed under the microscope with the focus adjusted right on the surface, a distinctly roughened image is observed on the silicon

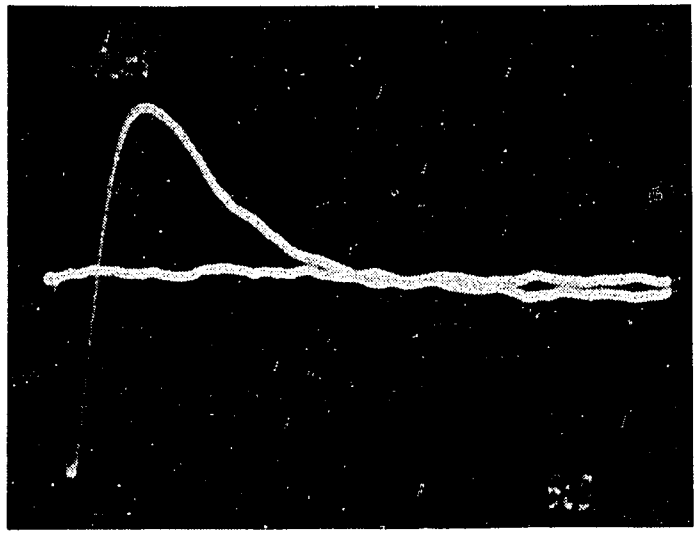

Figure 7. Beam deflection signal from a knife-edge/photomultiplier tube detector: sample, single crystal silicon wafer under vacuum; amount of material vaporized at each shot, 12 ng; sampling laser, Hyper EX 460 excimer laser at wavelength 308 nm, duration 25 ns, and energy 4.4 mJ/pulse

Figure 8. Photomicrograph of a crater generated by 177 superimposed laser exposures. The focal plane was on the top of the rim, 37 μm above the silicon target surface. The major and minor axes of the crater are 130 and 60 μm, respectively. Vaporization laser, Lumonics Hyper EX 460 excimer laser at 308 nm, 25 ns and 4.4 mJ/pulse

surface area exposed to only a single laser shot (Figure 9). There are indications that the surface layer has undergone a melting stage. The melting-flushing mechanism causes irragular roughening and the formation of outshoots. After the outshoots are formed, they reach higher temperatures and hence vaporize more readily than the flat surface. The fact that below certain laser irradiance, craters can only be formed after repeated exposures has been observed by other workers (44). The combined effect of melting, flushing, and condensation forms an annular rim 40 micrometers wide and 37 micrometers high around the crater. It was estimated from the photomicrographs that the porosity of the redeposited material was 80 %, which translates to 0.28 micrograms of condensed material. Therefore the ejected material was about 13 nanograms per pulse, in good agreement with the measurement by weight difference, 12 nanograms per pulse. Accordingly, it can be concluded that about 84 % of the material initially in the hole escaped from the surface. This represents a highly efficient vaporization process, which is one of the advantages expected from Q-switched UV lasers.

In the present measurement, the power density is about 10^9 W/cm^2. This value is above the threshold of silicon ionization (56), but the degree of ionization should be fairly low (57). This is implied by the numerical agreement of the calculated and experimental angles of deflection. As indicated by Eqn. (1), different components contribute differently to the overall index of refraction. When the power density is high, more atoms are ionized. Since k_e (electrons) is much higher than k_a (atoms) and k_i (ions), when the degree of ionization is higher

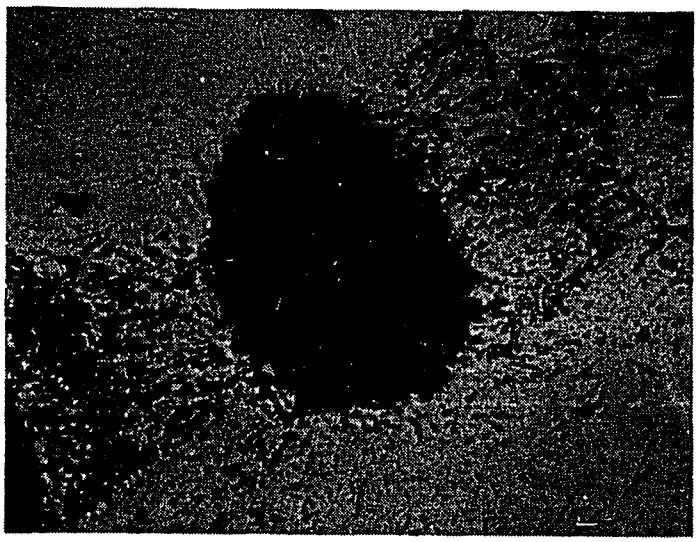

Figure 9. Photomicrograph of the same crater as that in Figure 8 with the focal plane right on the sample surface. The area adjacent to the right of the main crater was exposed to only a single laser shot where the evidence of surface roughening and phase transition can be observed. 84 % of the silicon originally in the crater was vaporized. The sputtered material can also be seen outside the crater

than a certain level, the experimental result becomes a good approximation of electron density. At an intermediate degree of ionzation, theoretically it is still possible to separate the $k_e N_e$ term from $k_a N_a$ and $k_i N_i$ terms, since they have a different wavelength dependence: k_e is proportional to the square of the wavelength of observation, while k_a and k_i vary only slightly through the whole visible region (58). These components, accordingly, can be separated by BD measurements made at two probe wavelengths. However, in order to employ this technique, some technical details must be taken into account.

Comparison of Beam Deflection and Interferometric Techniques in Laser Plume Diagnostics

Besides those electrostatic methods (59, 60) and spectroscopic methods (17, 19) for studies of laser plumes, interferometry has established itself as a standard method for density measurements (23). It is interesting to compare these two techniques because both are based on optical refractivity measurement, and both are capable of dealing with neutral and nonemitting species.

Interferometry measures the bulk index of refraction of the medium, and is ideal for those systems with long lightpaths and uniform density distributions. When multipass interferometers are used, e.g., Febry-Perot type, it is also suitable for those systems with slow temporal behavior because of the required transit time in the

interferometer cavity. Moreover, interferometry suffers from poor spatial resolution since it is difficult to have a small enough probe beam throughout the whole interferometer cavity.

The strength of beam deflection technique is evident in the study of laser plumes, the lightpaths of which are usually very small (~1 mm). In BD technique, what is measured is the gradient of refractive index rather than the bulk value, and the measurement can be finished in one pass; consequently, it is especially suited to systems with dramatic temporal variation. In beam deflection measurements, it is much easier to focus the probe beam into a small area within the tiny laser plume, which results in higher spatial resolution and higher sensitivity as well.

For the case shown in Figure 7, assuming that a spherical plume with a 1-mm diameter is formed from 12 ng silicon atoms, if the HeNe laser is used as the probe beam in interferometry, only a 0.1-fringe shift can be expected from the interferometric signal. It would be very difficult to extract density information from the resulant signal. Even though interferometric measurement can reach a sensitivity of 1/40 fringe shift by implementing phase analysis technique, the failure to focus the beam would cause different portions of the beam to see different atom number changes, resulting in different fringe shifts within the probe beam. As a consequence, it is very difficult to subtract any useful density information from the resulant signal. If the plume is 0.1 mm in size, then a 10-fringe shift can be expected; nevertheless, such measurement cannot be realized in practice because of

the rapid temporal variation and the extremely small physical plume dimension in comparison to the probe beam size.

To improve the spatial resolution, the size of the probe beam must be minimized. This can be done by using a Fabry-Perot interferometer with concave mirrors, by which the probe beam can be focused down to a small beam waist on the area under study (61). This geometry offers an additional advantage of better sensitivity than the parallel plane resonator (62). However, since the Fabry-Perot interferometers are of the multiple-pass type, the time resolution suffers when the event being studied is highly transient, such as plumes generated under vacuum by Q-switched lasers with short pulse duration. In addition, special caution should be exercised to protect the expensive interferometer mirrors from contamination from the ablated material.

Based on these considerations, for transient plumes with small physical dimensions, the BD technique is favored over interferometry when higher sensitivity, higher accuracy, and higher spatial and temporal resolutions are needed.

The BD Technique, however, suffers from more interferences. While interferometry is relatively immune to probe beam intensity fluctuations and any factor that causes attenuation of the beam, e.g., absorption, scattering, and blocking (35), BD measurements are highly sensitive to those factors. Pointing noise of the probe beam is another major noise source in BD studies. In addition, in a manner similar to the interferometric technique, the mechanical vibration and air turbulence are two sources of interference.

Conclusions

In summary, a new universal probe for transient atom sources has been demonstrated. Spatial and temporal density information can be obtained for electrically neutral species as well as charged species, and for nonemitting species as well as emitting species. The magnitudes and shapes of beam deflection signals are explained very well by a simple model. Individual vaporization events can be monitored, achieving a mass sensitivity of 1 ng on a silicon wafer. This method provides a direct and independent way to measure the expansion and vertical velocities of the ablated material. The effects of the crater shape on the expansion of the plume has been demostrated. Beam deflection also provides a new experimental approach to test different plume density models.

Since the magnitude of beam deflection signal is directly proportional to the amount of material vaporized, BD technique can be developed into a normalization method for laser microsampling. In the area of material processing, it can be used to monitor the etching rate under laser treatment. BD technique might find widespread use in other situations related to laser-solid interactions.

REFERENCES

1. Omenetto, N.; Winefordner, J. D. CRC Crit. Rev. Anal. Chem. 1981, 13(1), 59-115.

2. Laqua, K. In Analytical Laser Spectroscopy; Omenetto, N., Ed.; Wiley: New York, 1979; Chapter 2.

3. Piepmeier, E. H. In Analytical Applications of Lasers; Piepmeier, E. H., Ed.; Wiley: New York, 1986; Chapter 19.

4. Conzemius, R. J.; Capellen, J. M. Int. J. Mass Spectrom. Ion Phys. 1980, 34, 197-271.

5. Houk, R. S. In Analytical Applications of Lasers; Piepmeier, E. H., Ed.; Wiley: New York, 1986; Chapter 18.

6. Dittrich, K.; Wennrich, R. Prog. Anal. Atom. Spectrosc. 1984, 7, 139-198.

7. Rasberry, S. D.; Scribner, B. F.; Margoshes, M. Appl. Opt. 1967, 6, 87-93.

8. Van Deijck, W.; Balke, J.; Maessen, F. J. M. J. Spectrochim. Acta, Part B 1979, 34B, 359-369.

9. Brech, F. Appl. Spectrosc. 1962, 16, 59.

10. Krehl, P.; Schwirzke, F.; Cooper, A. W. J. Appl. Phys. 1975, 46, 4400-4406.

11. Pelah, I. Phys. Lett. 1976, 59A, 348-350.

12. Linlor, W. I. Appl. Phys. Lett. 1963, 3, 210-211.

13. Gilmour, A. S.; Giori, F. A. Presented at the 13th Annual Conference on Mass Spectrometry and Allied Topics, St. Louis, MO, May, 1965; paper 60.

14. Fenner, N. C.; Daly, N. R. Rev. Sci. Instr. 1966, 37,1068-1070.

15. Langer, P.; Tonon, G.; Floux, F.; Ducauze, A. IEEE J. Quantum Electron. 1966, QE-2, 499-506.

16. Sucov, E. W.; Pack, J. L.; Phelps, A. V.; Engelhardt, A. G. Phys. Fluids 1967, 10, 2035-2048.

17. MaLean, E. A.; Decoste, R.; Ripin, B. H.; Stamper, J. A.; Griem, H. R.; MaMahon, J. M.; Bodner, S. E. Appl. Phys. Lett. 1977, 31, 9-11.

18. Burgess, D. D.; Fawcett, B. C.; Peacock, N. J. Proc. Phys. Soc. (London) 1967, 92, 805-816.

19. Steenhoek, L. E.; Yeung. E. S. Anal. Chem. 1981, 53, 528-532.

20. Yappert, M. C.; Kimbrell, S. M.; Yeung. E. S. Appl. Opt. 1987, 26, 3536-3541.

21. David, C.; Avizonis, P. V.; Weichel, H.; Bruce, C.; Pyatt, K. D. IEEE J. Quantum Electron. 1966, QE-2, 493-499.

22. David, C. D. Appl. Phys. Lett. 1967, 11, 394-396.

23. Bruce, C. W.; Deacon, J.; Vonderhaar, D. F. Appl. Phys. Lett. 1966, 9, 164-166.

24. Yeung, E. S.; Steenhoek, L. E.; Tong, W. G.; Bobbitt, D. R. Anal. Chem. 1981, 53, 1936-1938.

25. Huie, C. W.; Yeung, E. S. Appl. Spectrosc. 1984, 38, 660-663.

26. Huie, C. W.; Yeung, E. S. Anal. Chem. 1986, 58, 1989-1993.

27. Kimbrell, S. M.; Yeung, E. S. Spectrochim. Acta, Part B 1988, 43B, in press.

28. Nolan, T. G.; Weimer, W. A.; Dovichi, N. J. Anal. Chem. 1984, 56, 1704-1707.

29. Jackson, W. B.; Amer, N. M.; Boccara, A. C.; Fournier, D. Appl. Opt. 1981, 20, 1333-1344.

30. Pawliszyn, J.; Weber, M. F.; Dignam. M. J.; Mandelis, A.; Venter, R. D.; Park, S. M. Anal. Chem. 1986, 58, 236-239.

31. Sell, J. A. Appl. Opt. 1984, 23, 1586-1597.

32. Pawliszyn, J. Anal. Chem. 1986, 58, 243-246.

33. Ascoli-Bartoli, U.; De Angelis, A.; Martellucci, S. Il Nuovo Cimento. 1960, 18, 4340-4361.

34. Casperson, L. W. Appl. Opt. 1973, 12, 2434-2441.

35. Lokhnygini, V. D.; Samokhin, A. A. Pis'ma Zh. Tekh. Fiz. 1975, 1, 749-752.

36. Gregg, D. W.; Thomas, S. J. J. Appl. Phys. 1966, 37, 4313-4316.

37. Saunders, P. A. H.; Avivi, P.; Millar, W. Phys. Lett. 1967, A27, 290-291.

38. Irons, F. E.; McWhirter, R. W. P.; Peacock, N. J. J. Phys. B.: Atom. Molec. Phys. 1972, 5, 1975-1987.

39. Haught, A. F.; Polk, D. H. Phys. Fluids 1966, 9, 2047-2058.

40. Fabbro, R.; Fabre, E.; Amiranoff, F.; Garban-Labaune, C.; Virmont, J.; Weinfeld, M.; Max, C. E. Phys. Rev. A. 1982, 26, 2289-2292.

41. Mandelis, A.; Royce, S. H. Appl. Opt. 1984, 23, 2892-2901.

42. Philipp, H. R.; Taft, E. A. Phys. Rev. 1960, 120, 37-38.

43. Thutupalli, G. K. M.; Tomlin, S. G. J. Phys. C., Solid State Phys. 1977, 10, 467-477.

44. Sato, T. Jpn. J. Appl. Phys. 1967, 6, 339-347.

45. Levinson, G. R.; Smilga, V. I. Kvant. Elektron. (Moscow) 1973, 3, 72-78.

46. Scott, R. H.; Strasheim, A. Spectrochim. Acta, Part B 1970, 25B, 311-332.

47. Bykovskii, Yu. A.; Kozyrev, Yu. P.; Sil'nov, S. M.; Sharkov, B. Yu. Kvant. Elektron. (Moscow) 1974, 1, 709-711.

48. Doschek, G. A.; Feldman, U. ; Burkhalter, P. G.; Finn, T.; A. Feibelman, W. A. J. Phys. B : Atom. Molec. Phys. 1977, 10, L745-748.

49. Putrenko, O. I.; Yankovskii, A. A. Zh. Prikl. Spektrosk. 1969, 11, 617-622.

50. Dawson, J. M. Phys. Fluids 1964, 7, 981-987.

51. Molmud, P. Phys. Fluids 1960, 3, 362-366.

52. Illingworth, R.; Thareja, R. K.; Raven, A.; Rumsby, P. T.; Stamper, J. A.; Willi, O. J. Appl. Phys. 1980, 51, 1435-1438.

53. Englehardt, A. G.; Phelps, A. V.; Sucov, E. W.; Pack, J. L. Bull. Am. Phys. Soc. 1966, 11, 464.

54. Felber, F. S.; Decoste, R. Phys. Fluids 1978, 21, 520-522.

55. Anisimov, S. I.; Rakhmatulina, A. Kh. Zh. Eksp. Teor. Fiz. 1973, 64, 869-876.

56. Kasuya, A.; Nishina, Y. Springer Ser. Chem. Phys. 1984, 36, 164-166.

57. Bloomfield, L. A.; Geusic, M. E.; Freeman, R. R.; Brown, W. L. Chem. Phys. Lett. 1985, 121, 33-37.

58. Alpher, R. A.; White, D. R. Phys. Fluids 1959, 2, 162-169.

59. Hirono, M.; Iwamoto, I. Jpn. J. Appl. Phys. 1967, 6, 1006.

60. Krehl, P. J. Appl. Phys. 1975, 46, 4400-4406.

61. Korobkin, V. V.; Malyutin, A. A. Zh. Tekh. Fiz. 1968, 38, 1095-1100.

62. Gerardo, J. B.; Verdeyen, J. T. Appl. Phys. Lett. 1963, 3, 121-123.

SECTION II

PHOTOACOUSTIC WAVE AS AN INTERNAL STANDARD FOR QUANTITATION OF LASER MICROPROBE ANALYSIS

INTRODUCTION

Limitations on the Precision of Laser Microsampling

The laser microprobe analyzer (LMA) was originally developed to enable qualitative analysis with high spatial resolution for solid samples of diverse nature, especially those electrically nonconducting and refratory samples. LMA has established itself as an appropriate tool for this purpose (1). Efforts have been made to improve its accuracy and reproducibility so that it can be used as a reliable quantitative tool; however, thus far this goal has not been fully realized.

Basically, the precision of trace analysis has its own statistical limitations. For trace analysis using LMA and conventional spectral apparatus, the precision of results from a single laser shot is limited by the small number of photons arriving at the detectors (2). However, when laser microprobe is used for solid sampling, the analytical precision of minor or even major components is still not comparable with that of solution samples.

The reason here is multifaceted. Firstly, as expected, the analytical precision is highly dependent on the reproducibility of the radiation parameters of sampling lasers including total power, pulse duration, power density, and its spatial and temporal variations. Among

these parameters, the power fluctuation on a shot-to-shot basis is the most important (3).

Secondly, matrix effects contribute to the irreproducibility of the results of analysis, though the use of lasers results in significant improvement over conventional methods like arcs and sparks in this respect (4, 5). This includes two factors, namely, physical and chemical matrix effects (6). The physical matrix effects refer to the influence exerted by the mechanical, physical, and also chemical nature of the sample surface in the vaporization process. The amount and forms of vaporized material depend on the absorption of laser radiation in the sample, which in turn, is dependent on the properties of the sample. Consequently, some of these factors may be summarized as internal metallurgical conditions such as grain size (7), mechanical tension (7), crystal orientation (8), and alloy structure (9). Other factors might include chemical composition (10), degree of sintering (in ceramic samples), etc. The chemical matrix effects, on the other hand, refer to the effects of foreign elements on the chemical composition or the total electron density of the plume, e.g., through chemical reactions between plume species. Not only the effective populations of the plume species in specific chemical forms are affected, but also their excitation and ionization states. As a result, both optical spectroscopic and mass spectrometric signals are affected. This effect is closely tied to the composition of the solid sample itself (11). In laser microprobe analysis, it has been found that the matrix effects are principally physical instead of chemical in nature (12).

Finally, as expected, variations in experimental conditions contribute to the irreproducibility of the analytical results. These include focusing and incidence angle of the vaporization laser (13); inhomogeneous distribution of vapor in the plume (14); and the surface condition changes due to etching, different sample surface treatment procedures (15), oxidation conditions, contamination, and so on.

If the intrinsic luminisity of the laser-generated plume is used for emission spectroscopic analysis, the quality of the emission spectra is usually poor. Besides, the material in the test sample is used inefficiently. Part of it is removed not as vapor, but in condensed phases (particulates and droplets) and, consequently, does not contribute to the characteristic spectroscopic signals. This is especially the case when the sample materials have low boiling points (16), and conventional-mode lasers are used for sampling (4). To alleviate this situation, further excitation is introduced (17). Among the excitation methods used so far, cross electrical discharge is most commonly adopted. By this technique, some atoms in ground state can be raised to excited states, and the retention time of the ablated material is increased; in addition, material in condensed phases (droplets and particulates) can undergo further vaporization and excitation. Thus, more free atoms contribute to the characteristic atomic emission signal. As a result of the auxiliary excitation, the spectral intensity is enhanced, and self-absorption as well as broadening is reduced (18). All these enable improvement of signal-to-background ratio by about an order of magnitude, better limit of detection is therefore possible.

Unfortunately, additional errors are introduced because of the temporal and spatial mismatch between the plume and the electrical discharge (14), the deposition of ablated material onto the electrodes, and the staining and contamination on the sample surface caused by the discharge; accordingly, the analytical precision gets worse, e.g., by a factor of three (6, 19). It has been found, however, that the error in sampling still constitutes the major source of irreproducibility when cross excitation is employed (20).

All the factors discussed above generally can not be precisely controlled; consequently, LMA remains so far only a qualitative or semiquantitative tool (6, 21), with relative standard deviation usually in the range of 10-30 %. For pellets of powdered materials, this value can be as high as 50 % for trace concentrations (22).

Techniques to Improve the LMA Reproducibility

Improved data reproducibility can be achieved by signal averaging over a number of laser pulses (19). However, the throughput suffers because multiple sampling becomes necessary. Moreover, spatial resolution, an inherent advantage of laser microprobe, no longer exist, since the region-dependent information is lost in the averaging process which involves multiple spots or depths. This method is hence not applicable to biological samples and other inhomogeneous solid samples.

Other alternatives have been suggested to improve the analytical

precision. These include using standard materials with closely matched chemical compositions (23), monitoring power fluctuation of the vaporization laser (24), measuring the size of the crater on sample surface produced by each laser shot (25), and using some kinds of internal references (26). Among these methods, the use of standard material is highly recommended to improve the analytical accuracy (27). It can not, however, take into account the variations of experimental parameters including the laser power fluctuation, so the improvement in precision is quite limited. Besides, it is not always possible to find a standard sample close enough in composition to that of the sample under study. Monitoring the laser power, unfortunately, results in no improvement in precision of analysis (24, 28), since the spectroscopic signals are not linear functions of laser power (29). Higher power does not necessarily produce a higher signal intensity; instead, it might make the event more violent, and generate more ions, especially multiply charged and more energetic ions (30). Besides, reflectivity and thus absorption of target material is intensity dependent (31). Exact measurement of crater size requires replication employing the Jarrell-Ash technique, and is therefore extremely tedious (22). The optical microscopic measurement, assuming that the crater is a right cone in shape, still takes several minutes (25) and cannot be done in situ. The minute amount of material removed by a single laser shot are often difficult to measure from the tiny crater, and large errors usually result. Moreover, this cannot take into account those droplets and clusters redepositing onto the sample or the cell wall, which are

ejected from the crater but do not contribute to the characteristic analytical signals (4).

The most useful technique among these is probably the use of an internal standard. In this scheme, the analyte emission line is paired with an emission line carefully chosen from a reference element, which is usually a matrix component. Then the analyte-to-standard intensity ratio is measured rather than the analyte line intensity itself (27). The assumption here is that interferences affecting the intensities of these two lines are identical. Although this is not always the case, as observed by Margoshes and coworkers (32), intensity ratio measurement in many cases does improve the reproducibility considerably (26, 27). Another assumption behind this method is that the reference elements selected are uniformly distributed over the whole volume of interest. This condition, however, cannot always be met. For instance, rocks and biological samples might represent quite contrasting cases. This method is also not applicable in inclusion analysis and depth profiling, where the volume of interest might have a quite different composition compared to the bulk. In addition, it is usually difficult to find an ideal internal reference element in biological and medical samples. On these occasions, other methods of normalization are definitely needed.

Since one of the useful characteristics of laser sampling is its relative freedom from evaporation selectivity, provided that power density of the vaporization laser is high enough to reach high plume temperature (33, 34). The basic question here is to choose a measurement which correlates directly to the amount of material created

by each laser shot in the desired form, e.g., atoms or vapor for atomic emission and absorption measurements. The selected physical parameter can then be used to normalize the intensity of the spectroscopic signal in each shot to yield better reproducibility. The density probe based on beam deflection, capable of monitoring the amount of material removed by an individual laser pulse (35), has the potential to serve this purpose.

Another normalization technique is demonstrated in the following. It is based on the volume change of the sampled material which undergoes sudden phase transition under intense laser pulse. By monitoring the photoacoustic wave associated with the plume generation, one should get an indication of the amount of material being sampled. The photoacoustic wave is detected by a microphone sensor located inside the sample cell, into which a buffer gas at a selected pressure is introduced. Under widely varying experimental conditions, the amplitude of the acoustic signal is compared with the emission intensities of both minor and major components in the sample. The results indicate that the precision of laser microprobe analytysis can be improved by using the acoustic wave as an internal standard.

EXPERIMENTAL SECTION

A block diagram of the instrumental arrangement is shown in Figure 1. A pulsed excimer laser (Lumonics, Ottawa, Canada, Model Hyper EX 460) running at the 308 nm XeCl transition was used as the vaporization laser. The UV beam was directed to the sample cell using a mirror (Newport, Fountain Valley, CA, 10QM20EM.15) and focused onto the sample surface using a planoconvex UV-grade quartz lens with 2" diameter and 150 mm focal length (Oriel, Stratford, CT). This lens was mounted on a micrometer translational positioner so that the focusing condition could be finely adjusted. The pulse energy used was regulated by varying the operating voltage and using variable apertures. The energy of each individual pulse was monitored by an energy ratiometer (Laser Precision, Utica, NY, Model Rj-7200) with an energy probe (Laser Precision, Utica, NY, Model RjP 734). The pulse duration was 25 nS and the repetition rate was typically 1 Hz. Actual sampling was done on time intervals much longer than one second to ensure thermal equilibrium of the surface with the surrounding buffer gas. Typical energy used in this work was less than 6 mJ/pulse. The pulse-to-pulse energy reproducibility was found to be ± 1.4 %.

The solid samples were cut into 1/4" x 1/8" x 1/16" pieces, and then mounted on the 45-degree inclined end surface of a stainless steel rod, which was screwed directly to a homemade micrometer 3D/tilt stage. The sample piece can hence be moved independently in three dimensions.

Figure 1. Experimental arrangement for simultaneous measurement of emission and acoustic wave associated with laser-generated plumes: A, aperture; C, sample cell; HV, high voltage power supply; L1, L2, planoconvex quartz lenses; M, mirror; MC, monochromator; MP, microphone; PA, preamplifier; PMT, photomultiplier tube; SA, solid sample; ST, 3D/tilt micrometer stage; VL, vaporization laser; WA, waveform analyzer

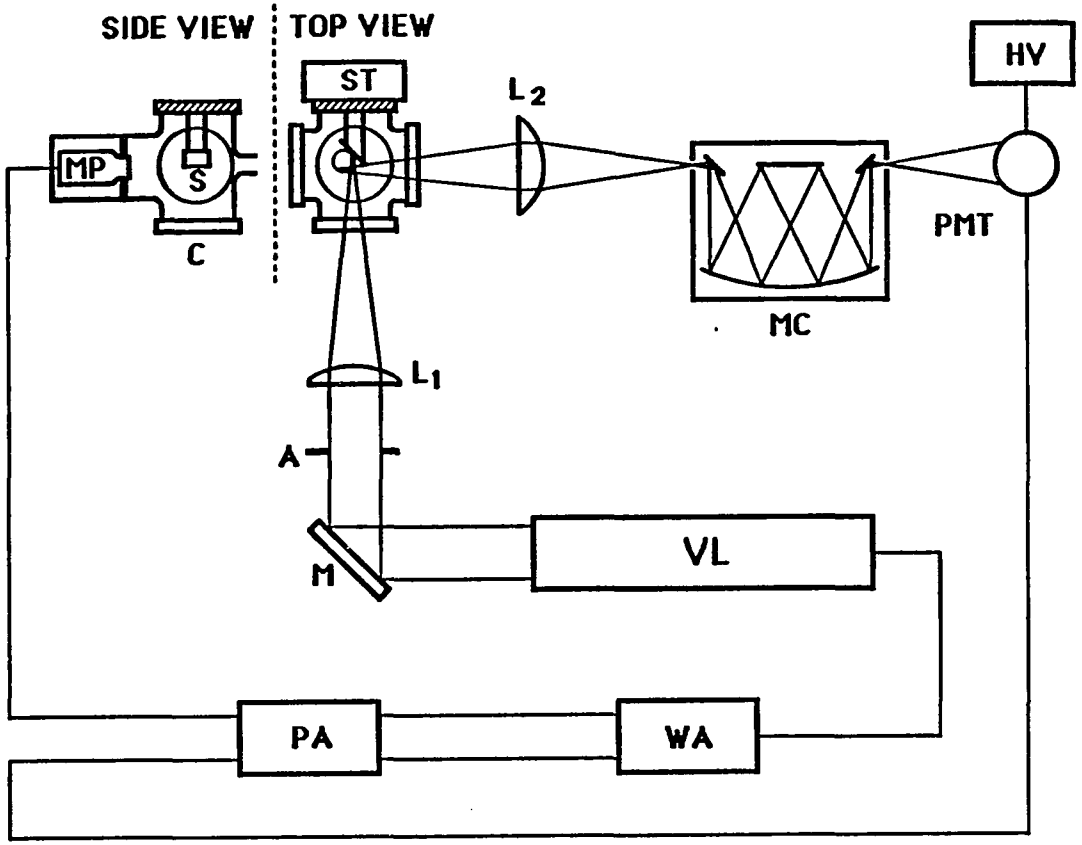
SIDE VIEW
TOP VIEW
ST
L2
HV
MP
S
C
PMT
MC
L1
A
M
VL
PA
WA

In this work, several pure metallic and alloy samples were used, including NBS SRM 1222 Cr-Ni-Mo steel, SRM C1150a white cast iron and SRM C1288 high alloy steel (National Bureau of Standards, Washington, DC). The sample surfaces were polished using #600 grit paper. Some were further ground on a Buehler polisher/grinder (Buehler, Lake Bluff, IL, Model Ecomat III) using Al_2O_3 polishing powders grade A and/or B with particle diameters 0.3 and 0.05 microns respectively. The sample surfaces were cleaned using organic solvents before the experiments. To ensure position reproducibility of the sample, a position reference bar was used which was defined by two precision pin-hole pairs. A new sample piece was glued on using 5-minute epoxy against a 45-degree groove in this bar and the original position recorded. A pyrex cell was mounted from the front against an O-ring to ensure airtightness. The cell was a cross in shape made from 2-cm diameter pyrex tubing. Quartz windows were attached to the ends of the tubing to introduce the pulsed UV laser beam and to monitor the emission. On the bottom of the cell a 0.5"-diameter condenser microphone (Knowles, Franklin Park, IL, Model BT-1759) was mounted to measure the photoacoustic wave associated with the laser plume. This type of microphone was used because of its relatively flat frequency response and hence suitability to measure impulse signals, and its insensitivity to mechanical vibrations (36). The cell volume (about 30 cm^3) was not minimized so as to avoid to certain extent the deposition of the ablated material onto the microphone diaphragm and the windows. The top of the cell was connected to a vacuum chamber so that a buffer gas at a selected pressure could be

introduced. A two-stage glass diffusion pump was used in the vacuum system. The chamber pressure was measured using a capacitance vacuum gauge (MKS Instruments, Burlington, MA, Type 221AHS-F-1000). Helium at 50 torr was used as the buffer gas.

In this work, a spatial masking scheme was employed. As shown in Figure 1, the continuum background emission from the crater area was blocked by the sample piece itself which was tilted at 45 degrees. Only the emission from the top periphery of the plume was collected by a planoconvex UV-grade quartz lens with 1" diameter and 3.5 cm focal length (Oriel, Stratford, CT), and imaged onto the entrance slit of a monochromator (PTR Optics, Waltham, MA, model ptr MC1-03). The monochromator had a f number of 4 and a reciprocal linear dispersion of 6 nm/mm. The wavelength reading was calibrated using a HeNe laser and several pure metallic samples. The slit width used in most cases was 150 microns. The emission intensity was recorded by a photomultiplier tube (Hamamatsu, Bridgewater, NJ, model R928). Because of the reproducibility of the sample in space, both masking conditions and light collection efficiency could be kept fairly constant from sample to sample, and from run to run. All the optical components were mounted on a 4' x 6' x 2" optical table (Newport, Fountain Valley, CA, Model NRC XS-46) padded with a 1/8" thick rubber sheet. To minimize the influence from those mechanical vibration sources, all mechanical pumps used in the same room were padded with 1-2" thick foam plastic sheets, and the bulky excimer laser was placed on another bench.

Both signals from PMT and microphone were sent to a two-channel waveform analyzer (Data Precision, Danvers, MA, Model D6000) via a two-channel preamplifier (Data Precision, Danvers, MA, Model D1000). The waveform analyzer had an 8-bit amplitude resolution and a sampling rate of 10 nS/point for one channel, or 20 nS/point for two channels. AC coupling mode was selected for all signal channels to reject the long-term noise. The peak area and height as well as other parameters were calculated by using the mathematical functions built in the waveform analyzer. Linear regression analysis was done on an IBM PC/AT personal computer using a Lotus 123 spreadsheet program.

RESULTS AND DISCUSSION

Optimization of Experimental Conditions

Laser sampling is often accompanied by plasma emission (37). While it might not be a problem in mass spectrometry and in cases where the plume is swept by an inert gas stream to another location for analysis, it causes severe interference to in-situ optical spectroscopic determinations. To minimize this continuous background, several approaches were taken in this work.

1) A UV laser at 308 nm was used as a vaporization laser. In laser mass spectrometry, the wavelength of the laser is not a primary parameter (38). It is relevant only because most metals absorb strongly in UV range, resulting in effective evaporation (39) and a shallow skin depth, defined as the light path by which the light intensity is attenuated to 1/e of its original value (40). A shallow skin depth is favored when depth resolution is an important parameter to consider. In optical spectroscopy, especially when measurements are done in situ, one has to deal with the interference from continuous plasma emission. Since the coefficient of inverse bremsstrahlung absorption, the major mechanism leading to plasma emission, decreases as the 2nd to 3rd power of the wavelength of the absorbed photons (41), short wavelength radiation minimizes plasma generation and couples better with solid

samples than long wavelengths. A reduced background continuum can then be expected (42).

2) A 45-degree angle of incidence was used to minimize the overlap and hence the interaction between the sampling laser beam and the plume, which ejects in a direction perpendicular to the sample surface (43). Enhancement in line-to-continuum ratio has been reported using this geometry (44, 45).

3) At pressures less than 100 torr, the main source of plasma emission is the plume itself (instead of the breakdown of gas medium), and is localized near the crater. The line emission, on the other hand, emits from a larger volume (13, 42, 46). Therefore, a spatial masking scheme was employed, by which the emission from the region near the crater was blocked by the inclined sample piece. Only the emission from the top periphery of the spherical plume was collected. This improved to some extent the line-to-background ratio (47).

4) The most intense part of the continuum lasts for a relatively short time, while the line emission persists much longer (microseconds) after the decay of the continuum emission (48, 49). This is shown in Figure 2, which was obtained using a # 4-96 color glass filter replacing the monochromator to block the lasing line. The spike with a time duration of about 1 microsecond shows no frequency dependence and corresponds, therefore, to the continuum plasma emission. The emission over a longer time period, on the contrary, can only be detected at the characteristic wavelengths and is hence from the line emission sources. Temporal differentiation (50, 51) is accordingly useful. This was also

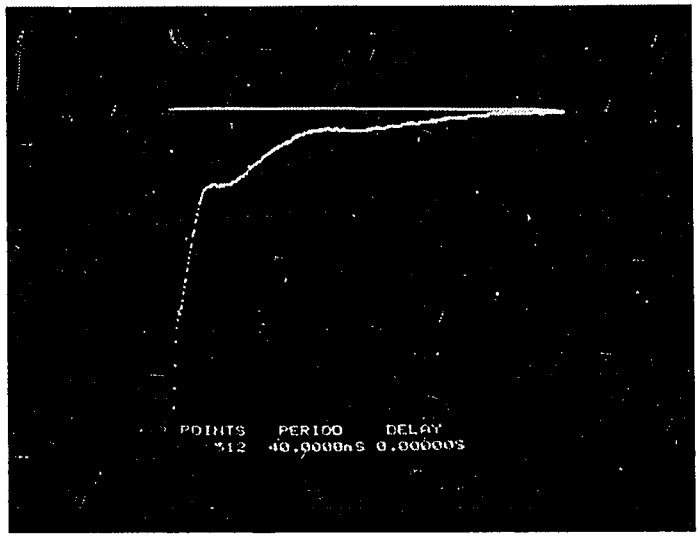

Figure 2. Temporal dependence of the continuous (plasma) emission (left peak) and line (atomic) emission (shoulders at the right). The start of the trace is synchronized with the laser pulse. Sample, NBS SRM 1222 Cr-Ni-Mo steel; laser, 308 nm, 25 ns, 0.95 ns/pulse; buffer gas, He at 50 torr; data sampling rate, 40 ns/point; #4-96 filter used without spatial masking

in part provided by the tilted sample itself, due to the time needed for the blown-off material to travel from the surface to the top periphery to become observable. The time involved can be estimated to be in microsecond time scale. In addition, time gating can be introduced easily in the waveform analyzer, so that the emission intensity can be integrated over a selected time segment.

5) Since the spectral characteristics of the plasma is continuous, the use of a monochromator proves necessary to reject the unwanted radiation.

6) For optical breakdown of gases under an intense radiation field, the power threshold increases with the decrease in gas pressure (52). It is, therefore, essential to keep the atmospheric pressure low, especially noting that the breakdown threshold of a gas decreases when it is in vicinity of a solid surface (53). Helium was used because of its relatively high breakdown threshold at reduced pressure.

7) Finally, it is essential to keep the power density low, since the ionization efficiency, governed by the Saha-Langmuir equation, is highly dependent on this parameter. Below 10^8 W/cm^2, the ion-to-neutral ratio is very low, of the order of 10^{-5}; on the contrary, at 5×10^9 W/cm^2, ionization efficiency can approach 100 % (38). In this work the power density was maintained to be less than 10^9 W/cm^2, as judged from the crater size.

The inert gas introduced into the cell couples the acoustic wave to the microphone. As a filler gas, helium gives a higher acoustic response than other gases under the same experiment conditions, owing to

its low heat capacity and high thermal conductivity (54). It has a second function of confining the plume to a small size (55), so the masking scheme mentioned above can be implemented. In addition, inert gases have been found to enhance the emission signal and reduce the continuous background (56). Lastly, its chemical inertness avoids the complication from potential chemiluminescent reactions between the plume and the atmospheric gas (57).

When the pressure is below 1 torr, the coupling efficiency is low and the acoustic signal is relatively weak and decays rapidly. The signal amplitude increases with pressure, because of the increase in coupling efficiency (58). At a pressure around 10 torr, it was found that the coupling efficiency increased sharply with laser power, resulting in an undesirable nonlinear response with respect to laser power. This is because the material evaporated (at high power) has a considerable contribution to the total pressure. The response tends to be linear at higher buffer pressures. But if the pressure approaches atmospheric pressure, complicated waveforms are observed. These result from rapid propagation, reflection, and mixing of the acoustic waves within the cell. Optical breakdown of the medium gas itself might also occur, leading to additional plasma emission. In view of these, the typical pressure within the cell was controlled at 50 torr.

The contribution of the sound wave transmitted through the solid media (sample mount and cell body, etc.) was found to be insignificant. Only minor peaks appeared in the time scale corresponding to the time needed to transmit the impulse from the sample surface to the microphone

through the solid path. This was also confirmed by the disappearance of acoustic peaks when the front path to the microphone was blocked by an aluminum disk. The acoustic wave observed, therefore, has two possible sources, namely, a density wave and a thermal wave. The former originates from material evaporated by the pulsed laser, i.e., an impulse generated by the explosive vaporization of ablated material from solid phase to form the plume. The latter, on the other hand, is due to heating of the solid and the buffer gas under the impact of laser radiation, and is hence independent of the vaporization process. Experimentally, these two components cannot be separated since they reach the microphone at about the same time. However, as discussed below, there is evidence that the density wave predominates in the detected acoustic wave.

Correlation between Photoacoustic and Emission Signals

The correlation between acoustic and emission signals associated with the laser-generated plume was investigated. These two signals were monitored simultaneously at different laser power, different focusing conditions, and different laser shots on various samples with different compositions, or treated by different procedures. A good linear correlation would imply that the acoustic signal could be used as an internal standard to normalize emission signals to achieve reliable quantitation. Emission was chosen for detection because of its

simplicity (no additional excitation light source was needed). The minor component Mn (< 1 %) in several iron and steel samples was selected as the analyte. The 403.1 nm Mn(I) line was used because it is intense and immune to interferences from Fe, Cr, Ti and Mo, the common matrix elements, at much higher concentrations (59). In fact, the fine-structure triplet around this wavelength was monitored as a whole, owing to line broadening and the limited resolving power of the monochromator used in this work. The emission peak area (EMPA) showed slightly better correlation to acoustic peak height (ACPH) than did emission peak height (EMPH). Therefore, the following results refer to ACPH-EMPA correlation unless specified otherwise. Shown in Figure 3 is a typical screen display on the waveform analyzer, the upper trace is the Mn(I) emission while the lower trace shows several early acoustic peaks. Among these peaks, the first narrow peak was found to have better correlation to the emission than the others. This is because it originates from the first impulse, without the complication from the wave reflection and mixing that followed. Hence, the results presented here refer to the first narrow peak. From these two signals, ACPH vs EMPA was plotted for different sets of experiment parameters, and the resulting correlation was evaluated by means of linear regression.

Figures 4 and 5 show the ACPH-EMPA correlation at varied laser focusing conditions at constant power. The top rightmost point was obtained when the UV laser beam waist was exactly on the sample surface. Each adjacent point corresponds to 0.5 mm movement of the focusing lens. It can be seen that efficient vaporization could be achieved only when

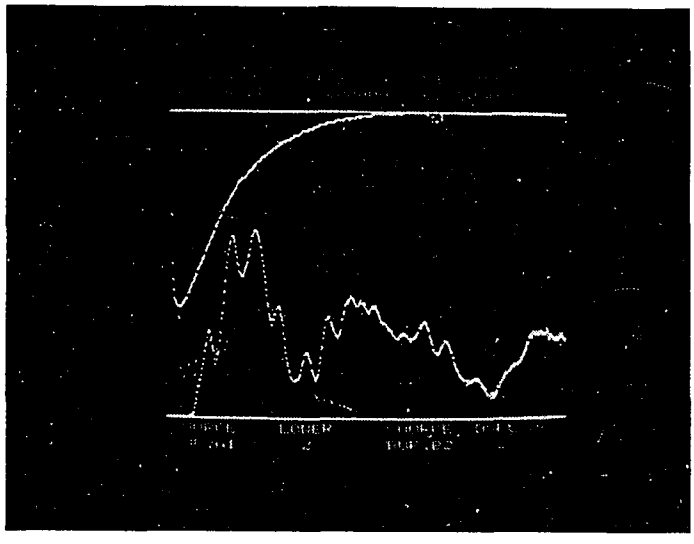

Figure 3. Waveform analyzer screen display. Upper trace, 403.1 nm Mn (I) emission at 40 ns/pt; lower trace, acoustic wave at 200 ns/pt. The start of the trace is synchronized with the laser pulse. Sample, NBS SRM C1288 high alloy steel; laser, 308 nm, 25 ns, 1 Hz, 1.2 mJ/pule; buffer gas, He at 50 torr

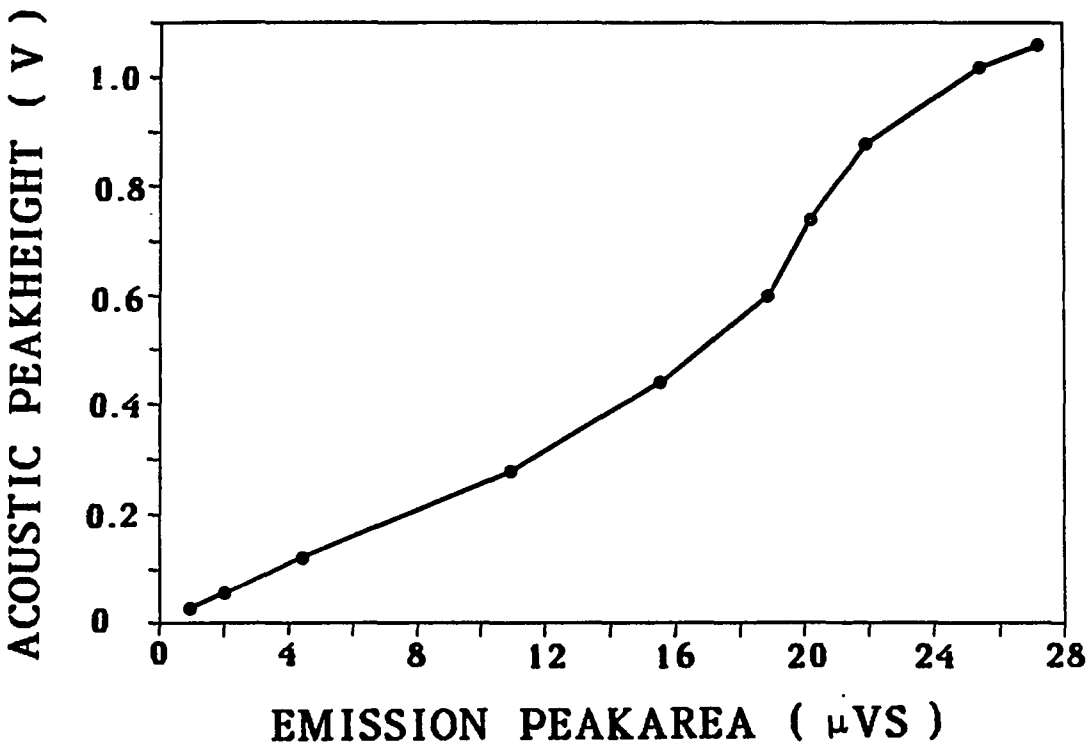

Figure 4. Acoustic peak height vs emission peak area at different focusing conditions. No time gating was applied to the emission signal. Sample, NBS SRM C1150a white cast iron; laser, 308 nm, 1 Hz, 25 ns, 5 mJ/pulse; buffer gas, He at 50 torr. The right most point corresponds to exact focusing. Each adjacent point corresponds to 0.5 mm movement of the focusing lens away from the sample surface

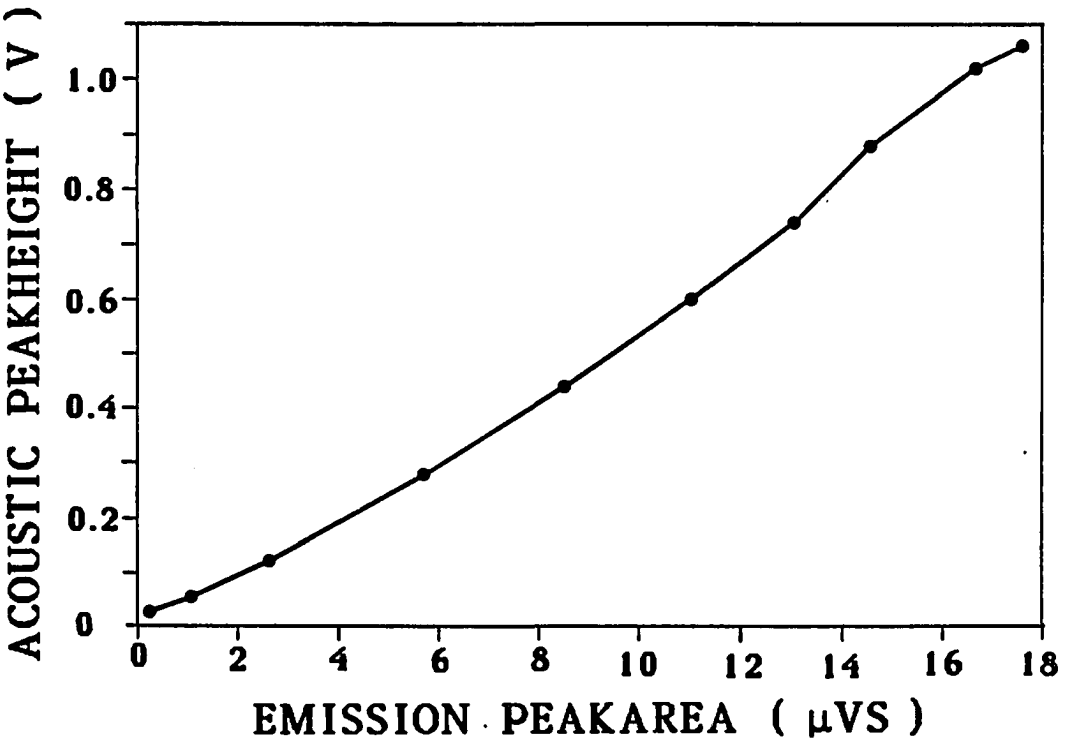

Figure 5. Acoustic peak height vs emission peak area (with time gating) for the same set of data as that in Figure 4. The emission signal was integrated over 1.6-20 μs.
R^2 = 0.9922

the power density was sufficiently high, i.e., when the focal point of the sampling laser is located less than 5 mm away from the target surface. When the focal point is above versus below the surface, heating of the plasma was achieved to a different extent, resulting in data that lie on two distinct lines. Only those points obtained with the focal point above the surface are shown in Figures 4 and 5. Figure 4 shows ACPH-EMPA correlation without time gating, while Figure 5 shows ACPH-EMPA correlation when the acoustic intensity was integrated only over the 1.6 to 20 microsecond time period. In the second case, good correlation (R^2 = 0.9922, R being the correlation coefficient) was obtained, whereas in the first case the data at high power density revealed higher acoustic response and lower emission intensity than those expected from a linear function. This can be explained by a higher degree of plasma formation under high laser power density at the very early stage of laser-target interaction (60). The absorption of laser energy by the plasma leads to attenuation of the laser beam reaching the target surface (61), and the generation of heat and hence thermal expansion of the plume. The consequences are weaker emission and stronger acoustic signal. At sufficiently high power density, the plasma can be heated to such an extent that it radiate light to the target surface (44) and cause additional vaporization. This might explain the fact that emission intensity increased again towards exact focusing. When the laser beam waist was moved away from the sample surface by 5 mm, both the emission and acoustic signals decreased by two orders of magnitude. Since the heating of the window, the buffer gas

and the solid matrix itself should not change much under the various focusing conditions, one can conclude that the acoustic wave components associated with these processes did not contribute significantly to the total acoustic signal. The impulse from the material vaporized off the surface should then be the dominant mechanism in acoustic wave generation. Based on Figure 5, in the experiments that follow, the laser beam waist was placed 2mm above the sample surface to avoid excess plasma emission.

The ACPH-EMPA correlation at different laser powers (fixed focus) was also studied using NBS SRM C1150a white cast iron. Under the experiment conditions similar to those in Figure 5, when the power was decreased gradually, both acoustic and emission signals lowered by more than two orders of magnitude, resulting in a good linear relationship with $R^2 > 0.99$. The dynamic range here is limited by microphone saturation at high power, and background noises at low power. The latter come from sources such as the thermal fluctuation of the buffer gas, ambient acoustic turbulences including mechanical vibrations from vacuum pumps, window heating, and electronic noise associated with the preamplifiers and the detection system (62). Linear correlation had been found for data extended over about three orders of magnitude but never beyond this range. Good correlation was found both for data from only the first laser shot ($R^2 = 0.9948$) (Figure 6) and for data from several superimposed shots on the same spot in the sample surface ($R^2 = 0.9939$) (Figure 7). These results imply that variations in emission due to laser power fluctuation can be properly corrected by simultaneously

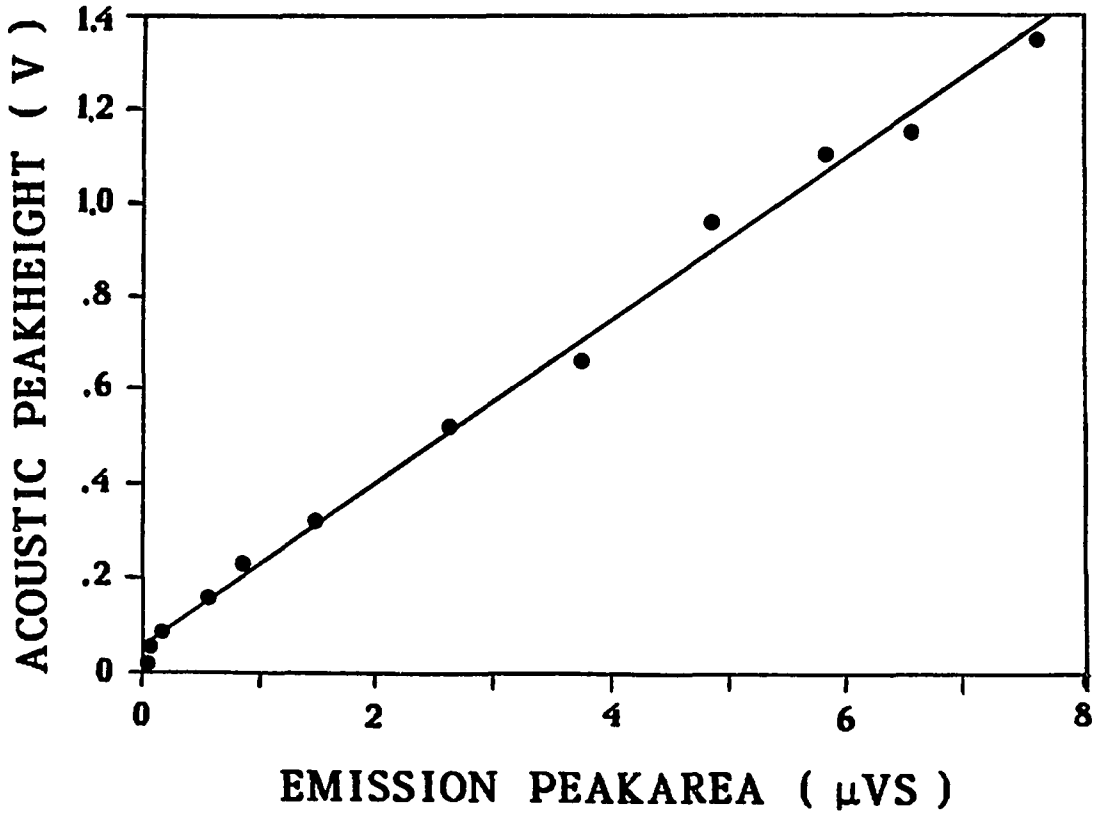

Figure 6. Acoustic peak height vs emission peak area at different laser power. Sample, NBS SRM C1288 high alloy steel; vaporization laser, 308 nm, 25 ns, 0.9-5.2 mJ/pulse; buffer, He at 50 torr. All data points were collected from the first exposure on different surface spots. R^2 = 0.9948. A different relative sample position here resulted in a slope different from those in other cases

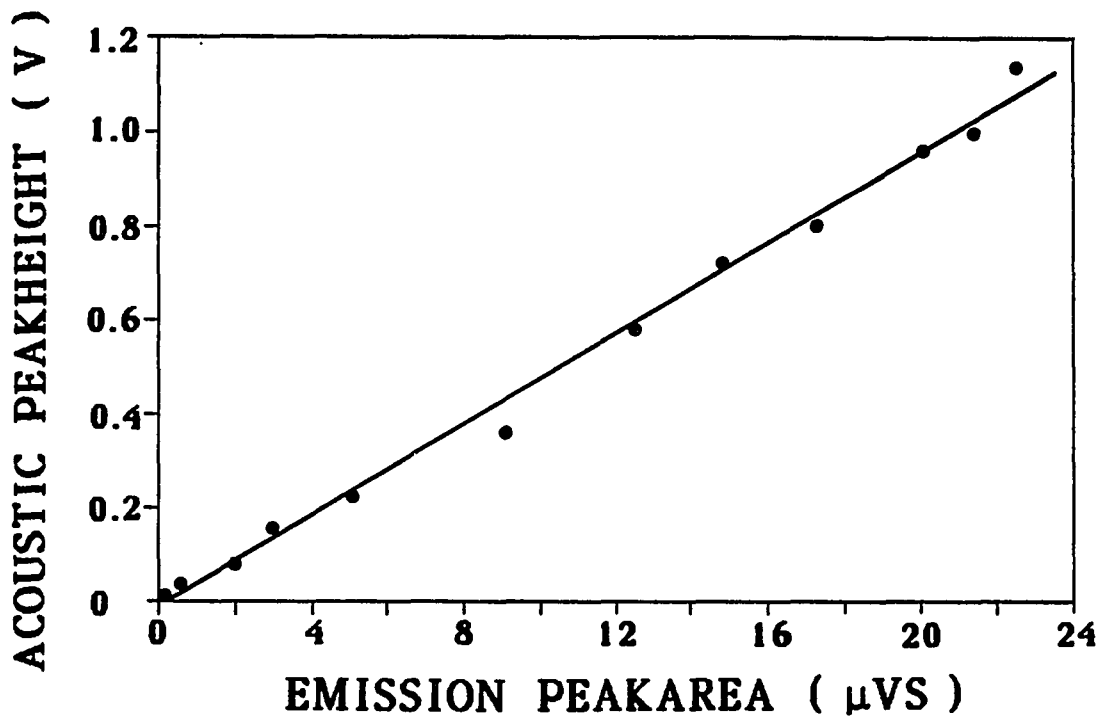

Figure 7. Acoustic peak height vs emission peak area at different laser power. Sample, NBS SRM C1150a white cast iron; vaporization laser, 308 nm, 25 ns, 0.4-2.3 mJ/pulse; buffer gas, He at 50 torr. All data points were collected from the consecutive exposures on the same spot. $R^2 = 0.9939$

monitoring the acoustic signal. Since laser power fluctuation is often the major error source in laser microprobe analysis, this observation might lead to significant improvement in LMA data precision.

To investigate the dependence of ACPH-EMPA correlation at widely varied surface conditions, data were collected for an extended series of superimposed laser shots on the same spot on the surface. During repeated laser exposures, the surface conditions of the irradiated spot changed drastically. A crater with an annular rim was formed as a result of vaporizition, melting, flushing, and resolidification (63). The decrease of the amount of ejected material after repeated laser exposures has been observed previously in other works, e.g., Ref. 35. The result is shown in Figure 8. The amount of material removed in each laser shot can be as little as 1 ng, and the fall was more drastic at the beginning of the exposure series. On account of these, data was collected at every shot at the very beginning of the series of vaporization events, with the collection interval gredually increased to every 30 shots at the end. The correlation was tracked for several hundred laser shots, during which both signals decreased more than an order of magnitude. A fairly good correlation (R^2 = 0.9710) was maintained. This is, however, a bit worse (large scatter from the line) than those in Figures 6 and 7. As the depth of the crater increases, confinement of the ejected plume occurs (35). One would expect the acoustic wave to be similarly affected. Again it could be seen that, in comparison to the acoustic wave component originating from vaporization, the components originating from heating of solid matrix and buffer gas

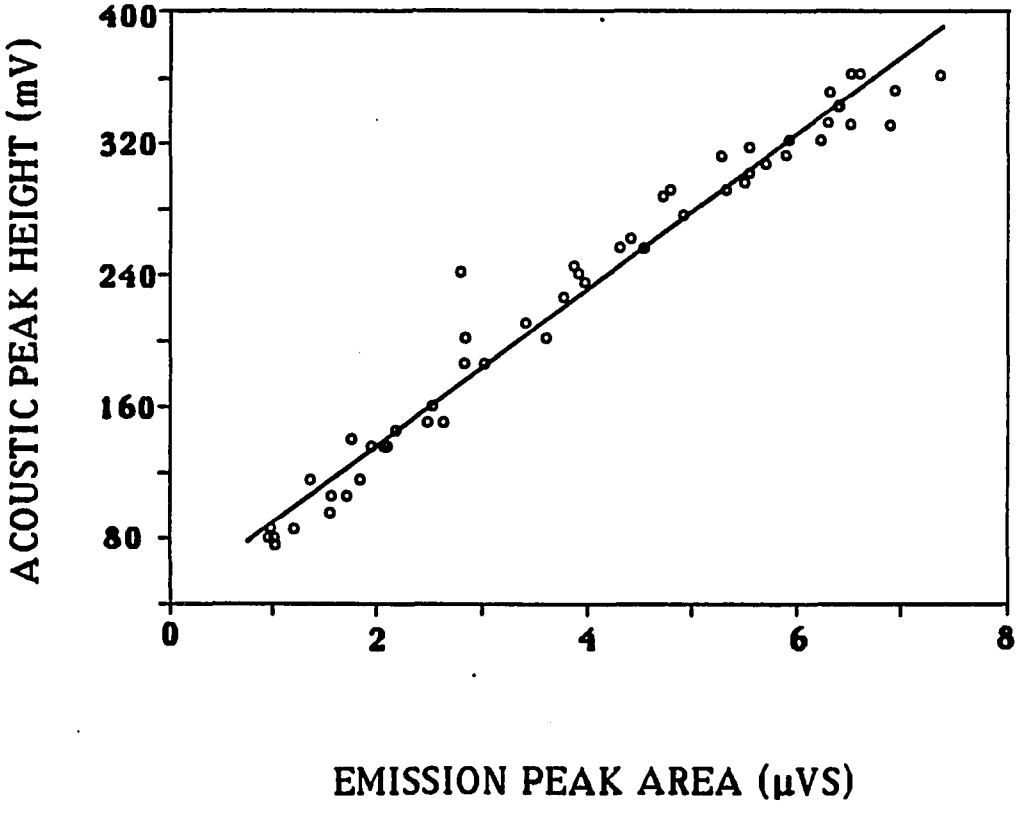

Figure 8. Acoustic peak height vs emission peak area at different laser shots on the same spot on sample surface. Sample, NBS SRM C1150a white cast iron; laser, 308 nm, 25 ns, 5 mJ/pulse; buffer gas, He at 50 torr; Data collection was performed at every shot at the beginning, then every 5-30 shots thereafter. A total of 430 shots were tracked. $R^2 = 0.9710$

were insignificant. This result, as well as those just mentioned above, implies that one can normalize the emission signal by monitoring the associated acoustic wave when focusing and surface conditions are varied to a significant extent. This should be especially useful in depth profiling, where it is extremely difficult to keep sample movement exactly in pace with the increase in the crater depth. Moreover, changes in surface conditions after repeated laser shots would inevitably cause the signal to vary, creating difficulty in doing even semiquantitative analysis. This might also make possible reliable laser microprobe analysis when the surface of solid samples can not be treated in a reproducible manner.

When the same experiments were made on two pieces of SRM C1288 high alloy steel treated in different ways (polished only, and further ground using grade A and B polishing powders with 0.3- and 0.05-micron diameter respectively), the two straight lines obtained showed similar slopes (0.0511 ± 0.0014 vs 0.0469 ± 0.0011 for about 50 data points each). It was found that SRM C1222 Cr-Ni-Mo steel and SRM C1150a white cast iron yielded slopes of similar values (0.0387 ± 0.0014 vs 0.0399 ± 0.0015 for about 50 data points each), indicating both samples have similar Mn contents (0.78 % vs 0.77 % in this case), even though the physical properties and chemical compositions of these two samples are quite different. On SRM C1288 high alloy steel with a similar Mn content of 0.83 %, however, a slope of 0.0469 was obtained under the same experimental conditions. Since the reciprocal of the slope is a measure of the Mn content, this unusually high slope indicates spectral

interference from the major component, Fe. SRM C1288 has an Fe content of 43 %, whereas the others have Fe contents of more than 90 %. This is a direct consequence of incomplete separation of the 403.1 nm Mn(I) triplet from adjacent Fe lines. As was mentioned in Ref. 59, the 403.1 nm Mn(I) line is immune to Fe interference at an analyte-to-concomitant ratio of 1:200, so that the difficulties associated with iron and steel analysis may be overcome by using a monochromator with higher resolving power. These results show that variations in the amount of sample vaporized due to matrix differences can be corrected to a certain extent by acoustic wave monitoring.

Good correlation (R = 0.994) was also found between the photoacoustic wave and the atomic emission from the major component. In this case, the Fe 386.0 nm line was monitored. This implies that the emission intensities of the major and the minor components are also correlated, so, the use of intensity ratios for normalization mentioned above (26, 27) is a good method whenever it can be implemented. Obviously, one has to assume that the major (reference) element is uniformly distributed, and that the two elements are excited equally. On the contrary, similar correlation could not be found between the photoacoustic signal and the continuous plasma emission. This is not surprising since the plasma is highly absorbing and is excited by complex mechanisms.

It is also interesting to note that very similar slope values were obtained on different samples with similar Mn contents under widely varied conditions. During the experiment process, red hot particles

could even be observed occasionally. It has been found that ejection of material in condensed phases, depending on target properties and laser ablation conditions, can play an important role in material removal process (4). These particles, without undergoing phase transition, actually contribute neither to atomic emission nor to acoustic signal. Therefore, unlike the method relying on crater size measurement (25), good correlation can still be maintained, regardless some material is removed as bigger particles or droplets.

Conclusions

Ultimately, it would be ideal to have a universal straight line by which all fluctuations in signal amplitude in laser microprobe analysis could be corrected, regardless of the experimental conditions and the nature of error sources. One must naturally exercise caution in using any one signal for normalization. In this work we have shown that the acoustic signal can track the emission signal linearly over three orders of magnitude. But, since the sampling laser used in this work had a fairly reproducible power output, with a relative standard deviation (RSD) of ± 1.4 %, improvement in shot-to-shot precision could not be demonstrated. This technique will be, however, especially valuable as an internal standard in LMA experiments where the laser output, sample conditions, and other experimental parameters vary substantially. These are the situations where normalization is most needed.

The photoacoustic wave, because of its origin, is a fairly direct indication of the amount of vapor phase produced under individual laser impact; as a result, acoustic wave monitoring is especially suitable for normalization of laser vaporization, regardless of whether the variation is due to physical matrix effects, or laser output fluctuations, or surface condition changes. This method, nevertheles, can not deal with chemical matrix effects. Fortunately, as mentioned previously, the LMA itself is usually free of chemical matrix effects (12, 64).

In this work only the emission signal was monitored, but the application of this normalization method could be extended easily to other spectroscopic techniques like atomic absorption (65), laser-induced fluorescence (66) and resonance ionization spectroscopy (67), as long as the inert gas atmosphere is allowed in the sampling compartment. This method is also applicable to the cases where the ablated material is swept by an inert gas flow to another location for observation (68) or further excitation (26), and to the cases where the ablated material is deposited onto a collector for saparate excitation (69).

This technique can be very useful in cases where it is difficult or even impossible to pair the analyte emission line with a reference line from a matrix element, such as analysis of medical and biological samples (70); and in cases where the area of interest has a composition very different from that of the bulk, such as analysis of biological and geological samples (71), and analysis of inclusions (72) and defects (73). In all these situations, normalization based on measurement of intensity ratio of analyte and reference lines cannot be implemented.

An intrinsit limitation on its usage stems from the buffer gas needed in the sampling compartment; consequently, this method is not suited to those thchniques where high vacuum is a necessity, like laser microprobe mass spectrometry.

REFERENCES

1. Laqua, K. In Analytical Laser Spectroscopy; Omenetto, N., Ed.; Wiley: New York, 1979; Chapter 2.

2. Leis, F.; Laqua, K. Spectrochim. Acta, Part B 1979, 34B, 307-316.

3. Rasberry, S. D.; Scribner, B. F.; Margoshes, M.; Appl. Opt. 1967, 6, 87-93.

4. Panteleev, V. V.; Yaskovskii, A. A. Zh. Prikl. Spektrosk. 1965, 3, 96-98.

5. Panteleev, V. V.; Petukh, M. L.; Putrenko, O. I.; Yankovskii, A. A. Zh. Prikl. Spektrosk. 1970, 13, 698-700.

6. Van Deijck, W.; Balke, J.; Maessen, F. J. M. J. Spectrochim. Acta, Part B 1979, 34B, 359-369.

7. Cerrai, E.; Trucco, R. Ener. Nucl. 1968, 15, 581-587.

8. Kirchheim, R.; Nagorny, U.; Maier, K.; Tolg, G. Anal. Chem. 1976, 48, 1505-1508.

9. Buravlev, Yu. M.; Morokhovskaya, I. I.; Murav'ev, V. N.; Nadezhda, B. P. Zavod. Lab. 1976, 42, 169-171.

10. Karn, F. S.; Singer, J. Fuel 1968, 47, 235-240.

11. Wennrich, R.; Dittrich. K; Bonitz, U. Spectrochim. Acta, Part B 1984, 39B, 657-666.

12. Marich, K. W.; Carr, P. W.; Treytl, W. J.; Glick, D. Anal. Chem. 1970, 42, 1775-1779.

13. Allemand, C. D. Spectrochim. Acta, Part B 1972, 27B, 185-204.

14. Moenke, H.; Moenke-Blankenburg, L.; Mohr, J.; Quifeldt, W. Microchim. Acta 1970, 6, 1154-1173.

15. Schroth, H. Fresenius Z. Anal. Chem. 1972, 261, 21-29.

16. Baldwin, J. M. Appl. Spectrosc. 1970, 24, 429-435.

17. Felske, A.; Hagenah, W. -D.; Laqua, K. Spectrochim. Acta, Part B 1972, 27B, 295-300.

18. Rasberry, S. D.; Scribner, B. F.; Margoshes, M.; Appl. Opt. 1967, 6, 81-86.

19. Felske, A.; Hagenah, W.-D.; Laqua, K. Spectrochim. Acta, Part B 1972, 27B, 1-21.

20. Whitehead, A. B.; Heady, H. H. Appl. Spectrosc. 1968, 22, 7-12.

21. Dittrich, K.; Wennrich, R. Prog. Anal. Atom. Spectrosc. 1984, 7, 139-198.

22. Wennrich, R.; Dittrich, K. Spectrochim. Acta, Part B 1982, 37B, 913-919.

23. Piepmeier, E. H. In Analytical Applications of Lasers, Piepmeier, E. H., Ed.; Wiley: New York, 1986; Chapter 19.

24. Peppers, N.; Scribner, E.; Alterton, L.; Honey, R.; Beatrice, E.; Harding-Barlow, I.; Rosan, R.; Glick, D. Anal. Chem. 1968, 40, 1178-1182.

25. Morton, K. L.; Nohe, J. D.; Madsen, B. S. Appl. Spectrosc. 1973, 27, 109-117.

26. Carr, J. W.; Horlick, G. Spectrochim. Acta, Part B 1982, 37B, 1-15.

27. Talmi, Y.; Sieper, H. P.; Moenke-Bankenburg, L. Anal. Chim. Acta 1981, 127, 71-85.

28. Saffir, A. J.; Marich, K. W.; Orenberg, J. B.; Treytl, W. J. Appl. Spectrosc. 1972, 26, 469-471.

29. Zahn, V. H.; Dietze, H. -J. Exp. Tech. Phys. 1972, 20, 401-408.

30. Houk, R. S. In Analytical Applications of Lasers; Piepmeier, E. H., Ed.; Wiley: New York, 1986; Chapter 18.

31. Basov, N. G.; Boiko, V. A.; Krokhin, O. N.; Semenov, O. G.; Sklizkov, G. V. Zh. Tekh. Fiz. 1969, 38, 1973-1975.

32. Margoshes, M.; Marcellus, D. A.; Rasberry, S. D. Proc. 13th Colloq. Spectroscopicum Internationale, Adam Hilger: London, 1968; pp 156.

33. Belousov, V. I. Zh. Anal. Khim. 1984, 39, 909-927.

34. Bykovskii, Yu. A.; Basova, T. A.; Belousov, V. I.; Gladskoi, V. M.; Gorshkov, V. V.; Degtyarev, V. G.; Laptev, I. D.; Nevolin, V. N. Zh. Tekh. Fiz. 1976, 46, 1338-1341.

35. Chen, G.; Yeung, E. S. Anal. Chem. 1988, 60, 864-868.

36. Schneider, A. J. Sound Vibr. 1970, 4 (Feb.), 20-25.

37. Carroll, P. K.; Kennedy, E. T. Contemp. Phys. 1981, 22, 61-96.

38. Conzemius, R. J.; Capellen, J. M. Int. J. Mass Spectrom. Ion Phys. 1980, 34, 197-271.

39. Fabbro, R.; Fabre, E.; Amiranoff, F.; Garban-Labaune, C.; Virmont, J.; Weinfeld, M.; Max, C. E. Phys. Rev. A. 1982, 26, 2289-2292.

40. Honig, R. E. J. Phys. Lett. 1963, 3, 8-11.

41. Browne, P. F. Proc. Phys. Soc. (London) 1965, 86, 1323-1332.

42. Piepmeier, E. H.; Osten, D. E. Appl. Spectrosc. 1971, 25, 642-652.

43. Knox, B. E. In Trace Analysis by Mass Spectrometry; Ahearn, A. J., Ed.; Academic Press: New York, 1972; Chapter 14.

44. Piepmeier, E. H.; Malmstadt, H. V. Anal. Chem. 1969, 41, 700-707.

45. Dimitrov, G.; Zheleva, Ts. Spectrochim. Acta, Part B 1984, 39B, 1209-1219.

46. Sucov, E. W.; Pack, J. L.; Phelps, A. V.; Englehardt, A. G. Phys. Fluids 1967, 10, 2035-2048.

47. Treytl, W. J.; Marich, K. W.; Glick, D. Anal. Chem. 1975, 47, 1275-1279.

48. Archbold, E.; Harper, D. W.; Hughes, T. P. Br. J. Appl. Phys. 1964, 15, 1321-1326.

49. Litvak, M. M.; Edwards, D. F. IEEE J. Quantum Electron. 1966, QE-2, 486-492.

50. Scott, R. H.; Strasheim, A. Spectrochim. Acta, Part B 1970, 25B, 311-332.

51. Treytl, W. J.; Orenberg, J. B.; Marich, K. W.; Glick, D. Appl. Spectrosc. 1971, 25, 376-378.

52. Minck, R. W. J. Appl. Phys. 1964, 35, 252-254.

53. Smith, D. C. J. Appl. Phys. 1977, 48, 2217-2225.

54. Adams, M. J.; King, A. A.; Kirkbright, G. F. Analyst 1976, 101, 73-85.

55. Kagawa, K.; Yokoi, S. Spectrochim. Acta, Part B 1982, 37B, 785-795.

56. Treytl, W. J.; Marich, K. W.; Orenberg, J. B.; Carr, P. W.; Miller, D. C.; Glick, D. Anal. Chem. 1971, 43, 1452-1456.

57. Beenen, G. J.; Piepmeier, E. H. Appl. Spectrosc. 1984, 38, 851-857.

58. Antipov, A. B.; Kapitanov, V. A.; Nikiforova, O. Yu.; Ponomarev, Yu. N.; Sapozhnikova, V. A. J. Photoacoust. 1983-1984, 1, 429-443.

59. Kriege, O. H.; Marks, J. Y.; Welcher, G. G. In Flame Emission and Atomic Absorption Spectroscopy, Vol. 3, Elements and Matrice; Dean, J. A., Rains, T. C., Ed.; Marcel Dekker: New York, 1975; Chapter 7.

60. Conzemius, R. J.; Zhao, S.; Houk, R. S.; Svec, H. J. Int. J. Mass Spectrom. Ion Phys. 1984, 61, 277-292.

61. Dymshitz, Yu. I.; Neverov, V. G. Pis'ma Zh. Tekh. Fiz. 1975, 1, 558-562.

62. Zharov, V. P.; Letokhov, V. S. In Laser Optoacoustic Spectroscopy; Springer Series in Optical Sciences, Vol. 37; Tamir, T., Ed.; Springer-Verlag: New York, 1984; Chapter 6.

63. Wagner, R. E. J. Appl. Phys. 1974, 45, 4631-4637.

64. Kwong, H. S.; Measures, R. M. Anal. Chem. 1979, 51, 428-432.

65. Manabe, R. M.; Piepmeire, E. H. Anal Chem. 1979, 51, 2066-2070.

66. Measures, R. M.; Kwong, H. S. Appl. Opt. 1979, 18, 281-286.

67. Mayo, S.; Lucatorto, T. B.; Luther, G. G. Anal. Chem. 1982, 54, 553-556.

68. Ka'ntor, T.; Bezur, L.; Pungor, E.; Fodor, P.; Nagy-Balogh, J.; Heincz, Gy. Spectrochim. Acta, Part B 1979, 34B, 341-357.

69. Adams, M. D.; Tong, S. C. Anal. Chem. 1968, 40, 1762-1765.

70. Marich, K. W. In Microprobe Analysis as Applied to Cells and Tissues; Hall, T., Echlin, P., Kaufmann, R., Ed.; Academic Press: New York, 1974; pp 15-31.

71. Keil, K.; Snetsinger, K. G. In Microprobe Analysis; Anderson, C. A., Ed.; John Wiley: New York, 1973; Chapter 13.

72. Korolev, N. V.; Faivilevich, G. A. Zavod. Lab. 1964, 30, 557-558.

73. Ryan, J. R.; Ruh, E.; Clark, C. B. Am. Ceram. Soc. Bull. 1966, 45, 260-262.

GENERAL SUMMARY

Two new techniques are described in this dissertation for diagnostics and normalization of laser-generated plumes, i.e., a density probe based on laser beam deflection, and the use of photoacoustic wave as an internal standard for quantitation of laser microsampling. These offer new experimental approaches for better understanding of laser-solid interactions, and might be useful for optimizing the laser vaporization, and finally developing the laser microprobe analysis into a reliable quantitative tool.

The beam deflection stems from the refractive index gradient, which is a direct result of a density distribution developed inside the plume during the expansion process. This technique is universal since the nature of the signal is one of optical refractivity. The probe beam can be focused onto a tiny spot in the plume, and generate a beam deflection in a single pass; as a consequence, the spatial and temporal resolutions are very high. Detectivity has reached 1 ng of total ejected material. For highly transient events with very small physical dimensions like laser plumes, this technique compares favorably to interferometry, althought both techniques are based on the same principle, i.e., optical refractivity.

For laser-generated plumes, this development adds a new technique to the diagnostics arsenal. Experimental results agree with the values calculated from a symmetrical expansion model with a radially linear

density distribution. Although a uniform density distribution has been observed interferometrically (41), theoretically it is the pressure gradient and hence density gradient that drives the radial plume expansion. It is therefeor reasonable to assume a linear density gradient inside the plume (107). Because of its excellent spatial and temporal resolutions, beam deflection technique offers a more reliable approach than interferometry to test experimentally those density models. Examples are the reciprocal square root profile suggested by Englehardt et al. (108), the exponential profile by Felber and Decoste (109), and that by Anisimov and Rakhmatulina which has an even more complicated function (110). The beam deflection signal contains the information about the overall geometry and density distribution of the plume, and its dynamics as well. From the BD signal, the vertical drift speed and the angle of plasma expansion, and the total ejected mass can be extracted. Accordingly, better insight is possible into laser-solid interactions in a broad sense.

For analytical chemists, this knowledge is highly useful for the optimization of laser vaporization, excitation, and subsequent spectroscopic or mass spectrometric observations as well. This will, undoubtedly, lead to more reliable analytical results. One of its immediate applications is to monitor the BD signal simultaneously with the spectroscopy signals, so that the latter can be corrected for the mass vaporized in each shot. The reproducibility of the latter can thus be improved. Some work has been done to investigate the correlation between the BD and the emission signals associated with the laser-

generated plumes. The best value of R^2 (square of correlation coeficient) obtained thus far has approached 0.75. It is considerably inferior to those in the photoacoustic wave cases; furthermore, it has been found that the BD signal itself is still not sufficiently reproducible for normalization purpose. Improvement might be expected by introducing a low atmospheric pressure to the sampling compartment to better confine the plume. This would, however, complicate the situation and hence the BD signal. Unfortunately, the basic restriction here might result from the generation of liquid droplets and particulates which accompanies the laser vaporization. As discussed in Ref. 111, these droplets and particles, situated in the laser light path, can cause attenuation of the beam intensity. This phenomenon has been observed under inefficient vaporization conditions, when sampling of silicon was performed using a longer-lasting, infrared carbon dioxide laser.

Governed by the Gradstone-Dale formula, all species in the plume contribute to the overall BD signal, in order to gain separate information on electrons as well as on atoms and ions, measurement must be done using two probe wavelengths. This is based on their different wavelength dependences, similar to what has been done on interferometry (94). The technical requirements here include obtaining two laser beams which are separated sufficiently in wavelength but overlapped well in space, so that the same spot of interest can be studied. This is not an easy task. The most likely approach might be to utilize two lasing lines from the same laser.

The BD technique might be well adopted in industrial fields where transient laser-solid interactions are involved, such as optimization and monitoring of laser machining and etching. Besides its use in density measurement and profile model testing, its other theoretical applications will definitely follow.

The BD technique, however, has its own restrictions. First of all, the plume must be transparent to the probe wavelength, so the plasma frequency must be lower than the probe beam frequency. This condition might not be satisfied for highly compact plumes with an electron density higher than the critical value, e.g., in the early stage of expansion. Secondly, as mentioned above, one should be cautious when ejection of droplets and particulates cannot be ignored in material removal.

The normalization of a laser microprobe using a photoacoustic signal as an internal standard, as described in Section II, is straightforward and can be done in real time. Fast in-situ normalization is thus possible. Theoretically, any variation in vaporization can be corrected, despite whether it is due to a physical matrix effect, the laser power fluctuation, or due to variations in surface and other experimental conditions. This method, though, cannot take into account the chemical matrix effects. Fortunately, this hardly constitutes any drawback, since the laser microprobe itself is fairly free of this interference (2, 112). This is in part due to the high temperature, the key to eliminating the chemical matrix effects (113), easily attainable in laser plumes (114); in part due to the streaming

motion of the ejected material, which drastically reduces the mutual interactions between the plume species (2).

Laser sampling, unfortunately, might be dominated by removal of material in condensed forms (droplets and clusters), especially when the boiling point of the specimen is low, or when a free-running laser is used. The mass ejected in condensed phases, as expected, does not emit at its characteristic wavelengths. Because of this, the correlation between crater size and spectroscopic signal is poor (115). Acoustic wave, on the contrary, is a more direct measure of the amount of vapor phase actually produced under individual laser impact. Accordingly, it can be a much more reliable normalization technique when the generation of droplets and clusters cannot be totally avoided. In addition, crater size measurement is impossible in depth profiling and in biological analysis. One should be careful, however, in applying this method to the two-step scheme, in which laser microsampling and subsequent excitation of the condensate are separated (35). Considerable error will definitely occur if the removal of droplets is the dominant process in laser sampling, which has been observed when a free-running laser is used (19).

In this work, only normalization of an emission signal was demonstrated. But application of this normalization scheme can be extrapolated easily to other spectroscopic techniques like atomic absorption (116), laser-induced fluorescence (32), and resonance ionization spectroscopy (36), as long as the inert atmosphere introduced is allowed in the sampling compartment. This method is, accordingly,

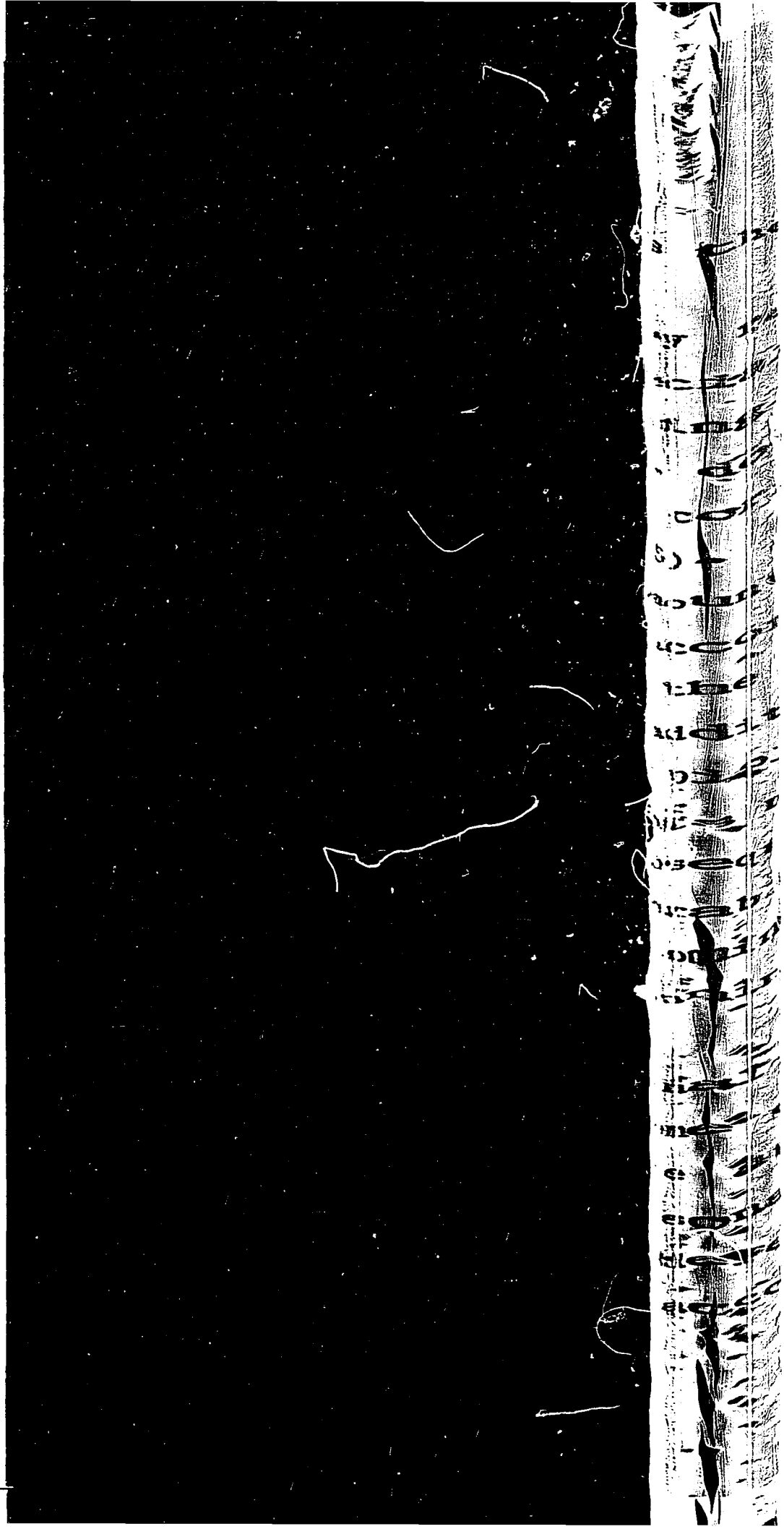

al

of

en the

is

. emit

on

tic

apor

y, it

ation

crater

l

to

or

rocess

er is

oduced

ly,

also applicable to the cases where the ablated material is swept by an inert gas stream to another location for observation (52), or further excitation (18).

The requirement of the buffer gas in the sample compartment would restrict to some extent the application of this method, especially in those occasions where a high vacuum level is a neccessity. As a result, its use in laser microprobe mass spectrometry is obviously excluded. However, some recent work has shown that the sampling can be done under enhanced pressure when it is separated from the subsequent ionization process (117, 118). This development makes possible the laser microprobe analysis of biological samples or even life organisms which undergo dehydration and denaturation under vacuum. This advance also opens the possibility of adopting the photoacoustic signal for the normalization of laser microprobe mass spectrometry.

REFERENCES

1. Chem. Eng. News 1971, 49 (July), 29-33.

2. Kwong, H. S.; Measures, R. M. Anal. Chem. 1979, 51, 428-432.

3. Reuter, W. Surface Sci. 1971, 25, 80-119.

4. Evans, C. A. Anal. Chem. 1972, 44 (13), 67A-80A.

5. Palmberg, P. W. Anal. Chem. 1973, 45, 549A-556A.

6. Brech, F. Appl. Spectrosc. 1962, 16, 59.

7. Southon, M. J.; Witt, M. C.; Harris, A.; Wallach, E. R.; Myatt, J. Vacuum, 1984, 34, 903-909.

8. Piepmeier, E. H. In Analytical Applications of Lasers, Piepmeier, E. H., Ed.; Wiley: New York, 1986; Chapter 18.

9. Houk, R. S. In Analytical Applications of Lasers, Piepmeier, E. H., Ed.; Wiley: New York, 1986; Chapter 19.

10. Klockenkampfer, R.; Laqua, K. Spectrochim. Acta, Part B 1977, 32B, 207-220.

11. Dittrich, K.; Wennrich, R. Prog. Anal. At. Spectrosc. 1984, 7, 139-198.

12. Belousov, V. I. Zh. Anal. Khim. 1984, 39, 909-927.

13. Opauszky, I. Pure Appl. Chem. 1982, 54, 879-887.

14. Devyatykh, G. G.; Maksimov, G. A.; Suchkov, A. I.; Larin, N. V. Zh. Anal. Khim. 1975, 30, 664-668.

15. Kohler, V. L.; Harris, A.; Wallach, E. R. In Microbeam Analysis-1986; Romig, A. D.; Chambers, W. F., Ed.; San Francisco Press: San Francisco, 1986, pp 467-470.

16. di Brozolo, F. R.; Odom, R. W. In Microbeam Analysis-1985, Armstrong, J. T., Ed.; San Francisco Press: San Francisco, 1985; pp 322-324.

17. Kagawa, K.; Yokoi, S. Spectrochim. Acta, Part B 1982, 37B, 789-795.

18. Carr, J. W.; Horlick, G. Spectrochim. Acta, Part B 1982, 37B, 1-15.

19. Boitsov, A. A.; Zil'bershtein, Kh. I. Spectrochim. Acta, Part B 1981, 36B, 1201-1213.

20. Van Deijck, W.; Blake, J; Maessen, F. J. M. J. Spectrochim. Acta, Part B 1979, 34B, 359-369.

21. Wennrich, R.; Dittrich, K. Spectrochim. Acta, Part B 1982, 37B, 913-919.

22. Felske, A.; Hagenah, W. -D.; Laqua, K. Spectrochim. Acta, Part B 1980, 35B, 731-740.

23. Rasberry, S. D.; Scribner, B. F.; Margoshes, M. Appl. Opt. 1967, 6, 81-86.

24. Felske, A.; Hagenah, W.-D.; Laqua, K. Spectrochim. Acta, Part B 1972, 27B, 1-21.

25. Mode, H. U.; Hagenah, W. D.; Laqua, K. Colloq. Spectrosc. Int. (Proc.) 15th, 1969, 4, 383.

26. Ishizuka, T.; Uwamino, Y. Anal. Chem. 1980, 52, 125-129.

27. Mitchell, P. G.; Sneddon, J.; Radziemski, L. J. Appl. Spectrosc. 1986, 40, 274-275.

28. Belliveau, J.; Cadwell, L.; Coleman, K.; Huwel, L.; Griffin, H. Appl. Spectrosc. 1985, 39, 727-729.

29. Thompson, J.; Goulter, J. E.; Sieper, F. Analyst 1981, 106, 32-39.

30. Mossotti, V. G.; Laqua, K.; Hagenah, W. D. Spectrochim. Acta, Part B 1967, 23B, 197-206.

31. Dittrich, K.; Wennrich, R. Spectrochim. Acta, Part B 1980, 35B, 731-740.

32. Measures, R. M.; Kwong, H. S. Appl. Opt. 1979, 18, 281-286.

33. Petukh, M. L.; Yankovskii, A. A. Zh. Prikl. Spektrosk. 1978, 29, 1109-1123.

34. Buravlev, Yu. M.; Nadezhda, B. P.; Babanskaya, L. N. Zavodsk. Lab. 1974, 40, 165-168.

35. Adams, M. D.; Tong, S. C. Anal. Chem. 1968, 40, 1762-1765.

36. Mayo, S.; Lucatorto, T. B.; Luther, G. G. Anal. Chem. 1982, 54, 553-556.

37. Conzemius, R. J.; Capellen, J. M. Int. J. Mass Spectrom. Ion Phys. 1980, 34, 197-271.

38. Glebov, G. D.; Iofis, N. A.; Chupina, M. S. Bull. Acad. Sci. USSR, Phys. Ser. (English translation) 1971, 35, 594-598.

39. Hercules, D. M.; Day, R. J.; Balasanmugam, K.; Dang, T. A.; Li, C. P. Anal. Chem. 1982, 54, 280A-305A.

40. Korolev, N. V.; Faivilevich, G. A. Zavodsk. Lab. 1964, 30, 557-558.

41. Klein, P.; Banatz, J. Fresenius Z. Anal. Chem. 1981, 308, 283-286.

42. Deloule, E.; Floy, J. F. Chem. Geol. 1982, 37, 191-202.

43. Ryan, J. R.; Ruh, E.; Clark, C. B. Am. Ceram. Soc. Bull. 1966, 45, 260-262.

44. Conzemius, R. J.; Svec, H. J. Anal. Chem. 1978, 50, 1854-1860.

45. Megrue, G. H. J. Geophys. Res. 1971, 76, 4956-4968.

46. Denoyer, E.; Natusch, D. F. S.; Surkyn, P.; Adams, F. C. Environ. Sci. Technol. 1983, 17, 457-462.

47. Giovannini, G. B.; Principato, G. B.; Rondelin, F. Anal. Chem. 1976, 48, 1517-1519.

48. Rosan, R. C.; Healy, M. K.; McNary, W. F. Science 1963, 142, 236-237.

49. Peppers, N. A.; Scribner, R. C.; Alterton, L. E.; Honey, R. C.; Beatrice, E. S.; Harding-Barlow, I.; Rosan, R. C.; Glick, D. Anal. Chem. 1968, 40, 1178-1182.

50. Chaplin, A. J.; Millard, P. R.; Schmidt, P. F. Histochemistry 1982, 75, 259-267.

51. Sullivan, R. C.; Pompa, C.; Sabatino, L. V.; Horan, J. J. J. Forensic Sci. 1974, 19, 486-495.

52. Ka'ntor, T.; Bezur, L.; Pungor, E.; Fodor, P.; Nagg-Balogh, J.; Heincz, Gy. Spectrochim. Acta, Part B 1979, 34B, 341-357.

53. McMahon, J. M. Lasers Appl. 1985, 4, 93-95.

54. Bloomfield, L. A.; Geusic, M. E.; Freeman, R. R.; Brown, W. L. Chem. Phys. Lett. 1985, 121, 33-37.

55. Huie, C. W.; Yeung. E. S. Anal. Chem. 1986, 58, 1989-1993.

56. Uglov, A. A.; Kokora, A. N.; Orekhov, N. V. Kvant. Elektron. (moscow) 1976, 3, 582-588.

57. Arata, Y.; Abe, N.; Oda, T.; Tsujii, N. In Plasma, Electron and Laser Beam Technology, Development and Use in Materials Processing, Arata, Y., Ed., American Society of Metals: Metals Park, OH, 1986, Chapter 5.

58. Bod, D.; Brasier, R. E.; Parks, J. Laser Focus 1969, 5 (Aug.), 36-38.

59. Kokora, A. N.; Romanov, G. S.; Stankevich, Yu. A.; Uglov, A. A. Fiz. i Khim. Obrab. Mater. 1987, 21, 54-61.

60. Lasers Appl. 1985, 4 (Aug.), 71-76.

61. Wolbarsht, M. L. IEEE J. Quant. Electron. 1984, QE-20, 1427-1432.

62. Yamanaka, C. Yokoyama, M.; Yamanaka, T.; Izawa, Y.; Tsuchimori, N. Lasers Opt. Non. Conv. 1967, 7, 54-56.

63. Basov, N. G.; Krokhin, O. N. Sov. Zh. Eksp. Teor. Fiz. 1964, 46, 171-175.

64. Laqua, K. In Analytical Laser Spectroscopy; Omenetto, N., Ed.; Wiley Interscience: New York, 1979; Chapter 2.

65. Bykovskii, Yu. A.; Basova, T. A.; Belousov, V. I.; Gladskoi, V. M.; Gorshkov, V. V.; Degtyarev, V. G.; Laptev, I. D.; Nevolin, V. N. Zh. Tekh. Fiz. 1976, 46, 1338-1341.

67. Basov, N. G.; Boiko, V. A.; Krokhin, O. N.; Semenov, O. G.; Skilizkov, G. V. Zh. Tekh. Fiz. 1968, 38, 1973-1975.

68. Shui, V. H.; Kivel, B.; Weyl, G. M. J. Quant. Spectrosc. Radiat. Transfer 1978, 20, 627-636.

69. Mott, N. F.; Jones, H. In The Theory of the Properties of Metals and Alloys; Dover Publications: New York, 1958; Chapter 3.

70. Ready, J. F. J. Appl. Phys. 1965, 36, 462-468.

71. Askar'yan, G. A.; Moroz, Ya. M. Zh. Eksperim. i Teor. Fiz. 1962, 43, 2319-2320.

72. Lokhov, Yu. N.; Mospanov, V. S.; Fiveiskii, Yu. D. Kvant. Elektron. (Moscow) 1974, 1, 385-389.

73. Spitzer, L. In Physics of Fully Ionized Gases; Interscience: New York, 1962; Chapter 5.

74. David, C. D.; Weichel, H. J. Appl. Phys. 1969, 40, 3674-3679.

75. Carroll, P. K.; Kennedy, E. T. Contemp. Phys. 1981, 22, 61-96.

76. Dymshitz, Yu. I.; Neverov, V. G. Zh. Tekh. Fiz. 1975, 1, 558-562.

77. Ready, J. F. In Effects of High-Power Laser Radiation; Academic Press: New York, 1971; Chapter 4.

78. Neilsen, P. E. J. Appl. Phys. 1979, 50, 3938-3943.

79. Arifov, T. U.; Askar'yan, G. A.; Tarasova, N. M. Zh. Eksp. Teor. Fiz., Pis'ma Red. 1968, 8, 128-132.

80. White, R. M. J. Appl. Phys. 1963, 34, 3559-3567.

81. Dregg, D. W.; Thomas, S. J. J. Appl. Phys. 1966, 37, 4313-4316.

82. Bykovskii, Yu. A.; Degtyarenko, N. N.; Elesin, V. F.; Kondrashov, V. E. Lovetskii, E.E.; Polyanichev, A. N.; Fetisov, V. S. Zh. Tekh. Fiz. 1974, 44, 73-82.

83. Kasuya, A.; Nishina, Y. Springer Ser. Chem. Phys. 1984, 36, 164-166.

84. Allemand, C. D. Spectrochim. Acta, Part B 1972, 27B, 185-204.

85. Ready, J. F. Appl. Phys. Lett. 1963, 3, 11-13.

86. Linlor, W. I. Appl. Phys. Lett. 1963, 3, 210-211.

87. MaLean, E. A.; Decoste, R.;Ripin, B. H.; Stamper, J. A.; Griem, H. R.; MaMahon, J. M.; Bodner, S. E. Appl. Phys. Lett. 1977, 31, 9-11.

88. Langer, P.; Tonon, G.; Floux, F.; Ducauze, A. IEEE J. Quantum Electron. 1966, QE-2, 499-506.

89. Honig, R. E. Appl. Phys. Lett. 1963, 3, 8-11.

90. Demtroder, W.; Jantz, W. Plasma Phys. 1970, 12, 691-703.

91. David, C.; Avizonis, P. V.; Weichel, H.; Bruce, C.; Pyatt, K. D. IEEE J. Quantum. Electron. 1966, QE-2, 493-499.

92. Bruce, C. W.; Deacon, J.; Vonderhaar, D. F. Appl. Phys. Lett. 1966, 9, 164-166.

93. David, C. D.; Weichel, H. J. Appl. Phys. 1969, 40, 3674-3679.

94. David, C.D. Appl. Phys. Lett. 1967, 11, 394-396.

95. Sucov, E. W.; Pack, J. L.; Phelps, A. V.; Engelhardt, A. G. Phys. Fluids 1967, 10, 2035-2048.

96. Saunders, P. H. A.; Avivi, P.; Millar, W. Phys. Lett. 1967, 24A, 290-291.

97. Steenhoek, L. E.; Yeung. E. S. Anal. Chem. 1981, 53, 528-532.

98. Ehler, A. W. J. Appl. Phys. 1966, 37, 4962-4966.

99. Feldman, U.; Doschek, G. A.; Behring, W. E.; Cohen, L. Appl. Phys. Lett. 1977, 31, 571-573.

100. Malvezzi, A. M.; Jannitti, E.; Tondello, G. Opt. Commun. 1975, 13, 307-310.

101. Basov, N. G.; Boiko, V. A.; Voinov, Yu. P.; Kononov, E. Ya.; Mandel'shtam, S. L.; Sklizkov, G. V. ZhETP Pis'ma 1967, 5, 177-180.

102. Izawa, Y.; Yamanaka, T.; Tsuchimori, N.; Yamanaka, C. Jpn. J. Appl. Phys. 1968, 7, 954.

103. Kimbrell, S. M.; Yeung, E. S. Spectrochim. Acta, Part B 1988, 43B, in press.

104. Bykovskii, Yu. A.; Degtyarenko, N. N.; Elesin, V. F.; Kozyrev, Yu, P.; Sil'nov, S. M. Zh. Eksp. Teor. Fiz. 1971, 60, 1306-1319.

105. Chen, G.; Yeung, E. S. Anal. Chem. 1988, 60, 864-868.

106. Chen, G.; Yeung, E. S. Anal. Chem. 1988, 60, 2258-2263.

107. Haught, A. F.; Polk, D. M. Bull. Am. Phys. Soc. 1966, 11, 464.

108. Englehardt, A. G.; Phelps, A. V.; Sucov, E. W.; Pack, J. L. Bull. Am. Phys. Soc. 1966, 11, 464.

109. Felber, F. S.; Decoste, R. Phys. Fluids 1978, 21, 520-522.

110. Anisimov, S. I.; Rakhmatulina, A. Kh. Zh. Eksp. Teor. Fiz. 1973, 64, 869-876.

111. Lokhnygini, V. D.; Samokhin, A. A. Pis'ma Zh. Tekh. Fiz. 1975, 1, 749-752.

112. Panteleev, V. V.; Yankovskii, A. A. Zh. Prikl. Spektrosk. 1965, 3, 96-98.

113. Kirkbright, G. F.; Sargent, M. Atomic Absorption and Fluorescence Spectroscopy; Academic Press: New York, 1974; Chapter 12.

114. Bogershausen, W.; Honle, K. Spectrochim. Acta, Part B 1969, 24B, 71-83.

115. Morton, K. L.; Nohe, J. D. Madsen, B. S. Appl. Spectrosc. 1973, 27, 109-117.

116. Manabe, R. M.; Piepmeier, E. H. Anal. Chem. 1979, 51, 2066-2070.

117. Holm, R.; Kampf, G.; Kirchner, D.; Heinen, H. J.; Meier, S. Anal. Chem. 1984, 56, 590-692.

118. Ishimori, A.; Yamamoto, T.; Yamada, T. In Microbeam Analysis-1986; Romig, A. D.; Chambers, W. F. Ed.; San Francisco Press: San Francisco, 1986; pp 473-474.

APPENDIX

BEAM DEFLECTION CAUSED BY INTERCEPTION WITH A SPHERICAL LASER-GENERATED PLUME WITH A RADIALLY LINEAR DENSITY PROFILE

The propagation of a Gaussian beam through a medium with spatially varying index of refraction n(r,t) is described by the paraxial equation:

$$\frac{d}{ds}\left(n_o \frac{dr_o}{ds}\right) = \nabla n(r,t) \qquad (1)$$

where s is the light path, r_o is the perpendicular displacement of the beam from its original direction, n_o is the uniform index of refraction, and $\nabla n(r,t)$ is the gradient of the refractive index perpendicular to the light path.

As has been described in Section I, when the duration of laser pulse is much shorter than the time of probe beam-plume interception, the plume is assumed to be created instantaneously. If vacuum is the background against which the plume expands, the plume undergoes simultaneously an isotropical radial thermal expansion and a perpendicular drift movement away from the target surface with velocity $\bar{v}$. When the probe beam is close to the target surface, the time of interception is short. During this observation period, both velocities of these motions can be approximated by constants. Under these

conditions, the plume dynamics at time t after the laser exposure can be depicted in Figure 1, where h is the probing height, is the total angle of deflection caused by the beam-plume interception, and is the angle of expansion. The radius of the plume R is

$$R = vt \sin \alpha \tag{2}$$

In this work, the radial density distribution is approximated by a linear profile, which can be described as

$$N^r = \left(1 - \frac{r}{R} \right) N^o \qquad (0 \leq r \leq R) \tag{3a}$$

$$N^r = 0 \qquad (r > R) \tag{3b}$$

where N^r is the number density inside the plume at a distance r away from the center of the plume, O, and N^o is the number density at the center of the plume. The total number of particles N_o can then be calculated by integrating N^r over the whole sphere:

$$N_o = \int_0^R \left(1 - \frac{r}{R} \right) N^o (4 \pi r^2) \, dr = \frac{\pi}{3} N^o R^3 \tag{4}$$

From this, the maximum density at plume center O at time t can be expressed as

$$N^o = \frac{3N_o}{\pi R^3} = \frac{3N_o}{\pi (vt \sin \alpha)^3} \tag{5}$$

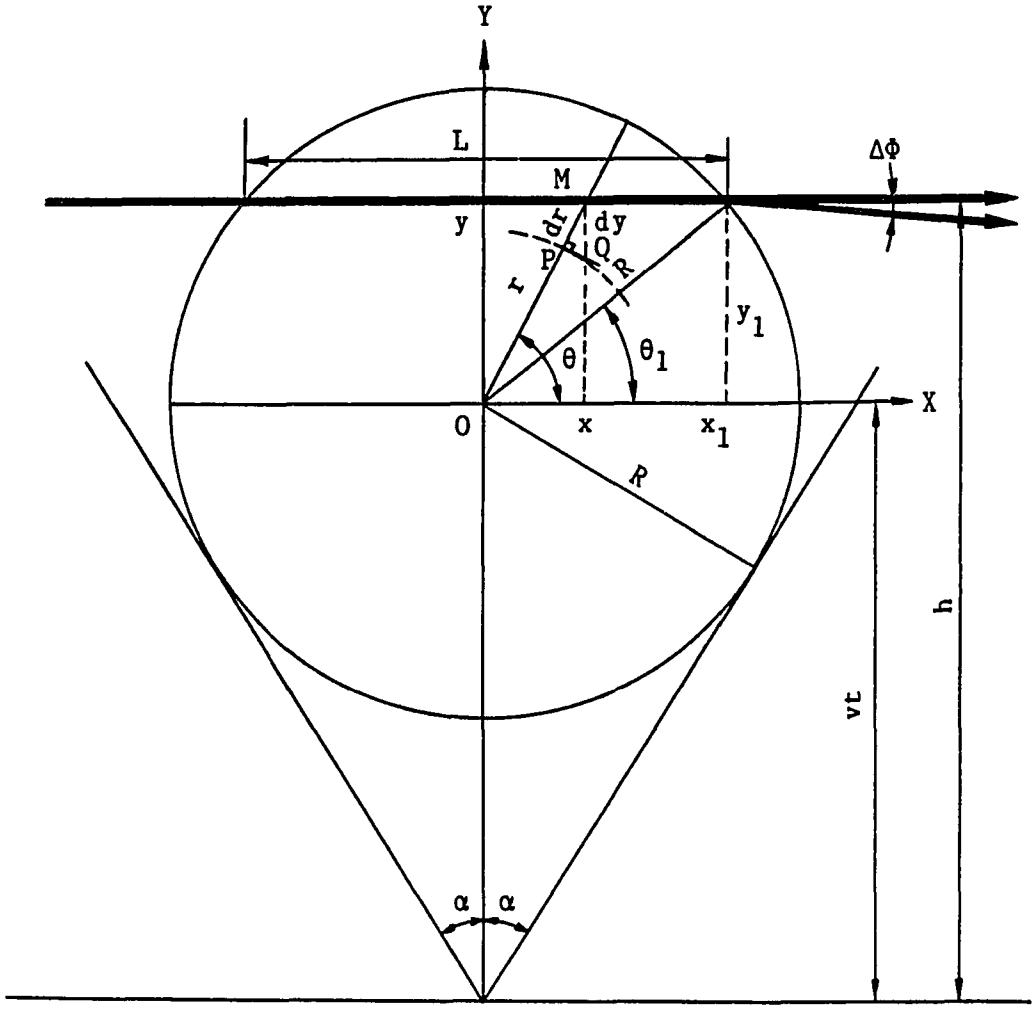

Figure 1. Beam deflection caused by interception with a spherical plume with a radially linear density profile

The refractive index of a gaseous medium with i components is given by the Gradstone-Dale formula:

$$n - 1 = \sum_{j=1}^{i} k_j N_j \tag{6}$$

where n is the refractive index of the medium, N_j is the number density of the jth component, and K_j is the specific refractivity of the jth component. When the degree of ionization is low, the contributions from the charged particles are negligible. Then Eqn. (6) can be simplified as

$$n = 1 + k\, N^r \tag{7}$$

For any point M inside the plume along the light path, one has

$$\sin \theta = \frac{h - vt}{r} \tag{8}$$

where θ is the angle between the radius OM and the horizontal plane. The refractive index n at position M is given by

$$n = 1 + kN^r = 1 + k \left(1 - \frac{r}{R} \right) N^o \tag{9}$$

Therefore,

$$\frac{dn}{dr} = - \frac{N^o k}{R} \tag{10}$$

In the triangle MPQ, for any increment dr, the corresponding increment dy is given by

$$dy = \frac{dr}{\sin \theta} \tag{11}$$

The density gradient perpendicular to the light path is therefore

$$\frac{dn}{dy} = \frac{dn}{dr}\frac{dr}{dy} = -\frac{N^{o}k}{R}\sin\theta \tag{12}$$

To carry out the calculation, Eqn. (1) can be rewritten as

$$\frac{\partial \Phi}{\partial x} = \frac{1}{n}\frac{\partial n}{\partial y} \tag{13}$$

and the angle of deflection $\Delta\Phi$ can be obtained by integrating $\frac{1}{n}\frac{\partial n}{\partial y}$ over the light path L:

$$\Delta\Phi = \int_{0}^{L} \frac{1}{n}\frac{\partial n}{\partial y}\,dx \tag{14}$$

For gaseous medium, $n \approx 1$. This is especially true when the amount of material ablated in each laser exposure is very tiny. So 1/n can be approximated by 1, therefore, the above integral becomes

$$\Delta\Phi = 2\int_{0}^{x_1} \frac{\partial n}{\partial y}\,dx \tag{15}$$

The integration can be carried out by converting the Cartesian coordinate to the spherical coordinate as follows:.

$$x = y \cot \theta = R \sin \theta_1 \cot \theta \tag{16}$$

$$dx = R \sin \theta_1 \, d(\cot \theta) = - \frac{R \sin \theta_1}{\sin^2 \theta} d\theta \tag{17}$$

By substituting (12) and (17) into (15), and carrying out the integration, the expression for the angle of deflection is finally obtained:

$$\Delta\Phi = \frac{6N_o k (h - vt)}{\pi (vt \sin \alpha)^4} \ln \left\{ \tan \left(\frac{1}{2} \arcsin \left(\frac{h - vt}{vt \sin \alpha} \right) \right) \right\} \tag{18}$$

in which $\Delta\Phi$, N_o, v, and h can be measured experimently. α can be obtained directly for emitting species, or indirectly by curve fitting for nonemitting species. The total angle of deflection, therefore, can be calculated and compared with the experimental result.

ACKNOWLEDGEMENTS

This work was performed at Ames Laboratory under contract No. W-7405-eng-82 with the U. S. Department of Energy. The United States government has assigned the DOE Report number IS-T-1403 to this thesis.

First of all I want to thank Dr. Edward S. Yeung, my major professor, who opened the door for me to the fascinating world of laser spectroscopy, for his expert guidance throughout the research projects. His dedication to science, enlightening teaching and understanding are good examples for me.

I want to thank the professors who served on my committee: Robert Angelici, Dennis Johnson, Robert Houk, Glenn Schrader, and Walter Struve. They devoted their precious time to help me finish all the tedious work during this program.

Being in a stimulating research group is a good memory to me. I would like to thank all my fellow graduate students and postdocs, who gave me so much help during years in Iowa State. They were so considerate in sharing equipment, space, and so enthusiastic in sharing their knowledge and experience. I feel fortunate to be a member in this group.

I am grateful to Gary Wells, Harry Amenson, and Tom Johnson in Ames Lab Student Machine Shop, who helped me so much in machining; to H. S. Hall and C. L. Patterson in Chemistry Glass Blowing Shop, who made

most of the glassware; and to Dr. Scott Chumbley in Metallurgy Department, who helped me to take the photomicrographs.

I also want to express my appreciation to my friends here in Ames, who gave my family so much help, and made life in this peaceful town a good memory: Emily and Steve Skaar, Anne and Shuming Huang, Jane and Richard Lamb, Elsie and Marleo Parter, and Robin and Bill Nichols.

Anna Yeung, who creates a warm and friendly atmosphere for the whole group, deserves special thanks.

My mother, with her unsurpassed love and support for my education; and my mother-in-law, who had been taking care of Jie, my daughter, with all her love, deserve special thanks and praise.

Finally, I would like to express my gratitude, from the bottom of my heart, to my wife, Hui Liu, for her love, and her effort to take care of Jie when we were separated. This work would have been impossible without her support.